NASA CR-171985

HOLLOW CATHODE PLASMA COUPLING STUDY - 1986

Prepared For

JOHNSON SPACE CENTER

NATIONAL AERONAUTICS AND SPACE ADMINISTRATION

Grant NAG 9-120

(NASA-CR-171985) HOLLOW CATHODE PLASMA COUPLING STUDY, 1986 Annual Report, 1 Aug. 1985 - 1 Aug. 1986 (Colorado State Univ.) 84 p Avail: NTIS HC A05/MF A01 CSCL 09C

N88-11949

G3/33 Unclas 0106772

Annual Report

December 1986

Paul J. Wilbur
Department of Mechanical Engineering
Colorado State University
Fort Collins, CO 80523

TABLE OF CONTENTS

LIST OF FIGURES

INTRODUCTION

A space plasma contactor is a device designed to make a low impedance electrical connection between some point in an instrument or on a spacecraft surface and an adjacent space plasma. It serves essentially the same function as the electrical grounding wire used in terrestrial applications and in so doing it can provide both the desired reference potential and prevent spacecraft charging. The effectiveness of the plasma contactor becomes especially important when large currents are flowing in a space-based system as they will be in the case of the electrodynamic tether system.[1] The work described here is directed at developing and understanding plasma contactors which will eventually be useful in the high current applications associated with electrodynamic tether operation.

Typically an electrodynamic tether system includes two space vehicles connected by a long conductive wire or tether as suggested by the sketch in Fig. 1. When properly oriented the tether will cut across geomagnetic field lines as it moves in orbit and as a result a voltage difference will be induced between its two ends. In order to take advantage of this voltage difference for direct current power generation purposes a return path for the current that could flow from one end of the tether to the other through an electrical load must be provided. Figure 1 shows a scheme proposed to provide this return path through plasma contactors and the ionosphere. Efficient power generation is achieved with this system if the load impedance is large compared to the sum of the impedances of the other elements in the current, i.e. the tether resistance, ionospheric impedance and the impedances of the two plasma contactors. As Fig. 1 suggests, two plasma contactors are required, one collecting electrons (and emitting ions) and the other one emitting electrons (and collecting ions). Electrons which move much more rapidly than ions at a given energy, would be

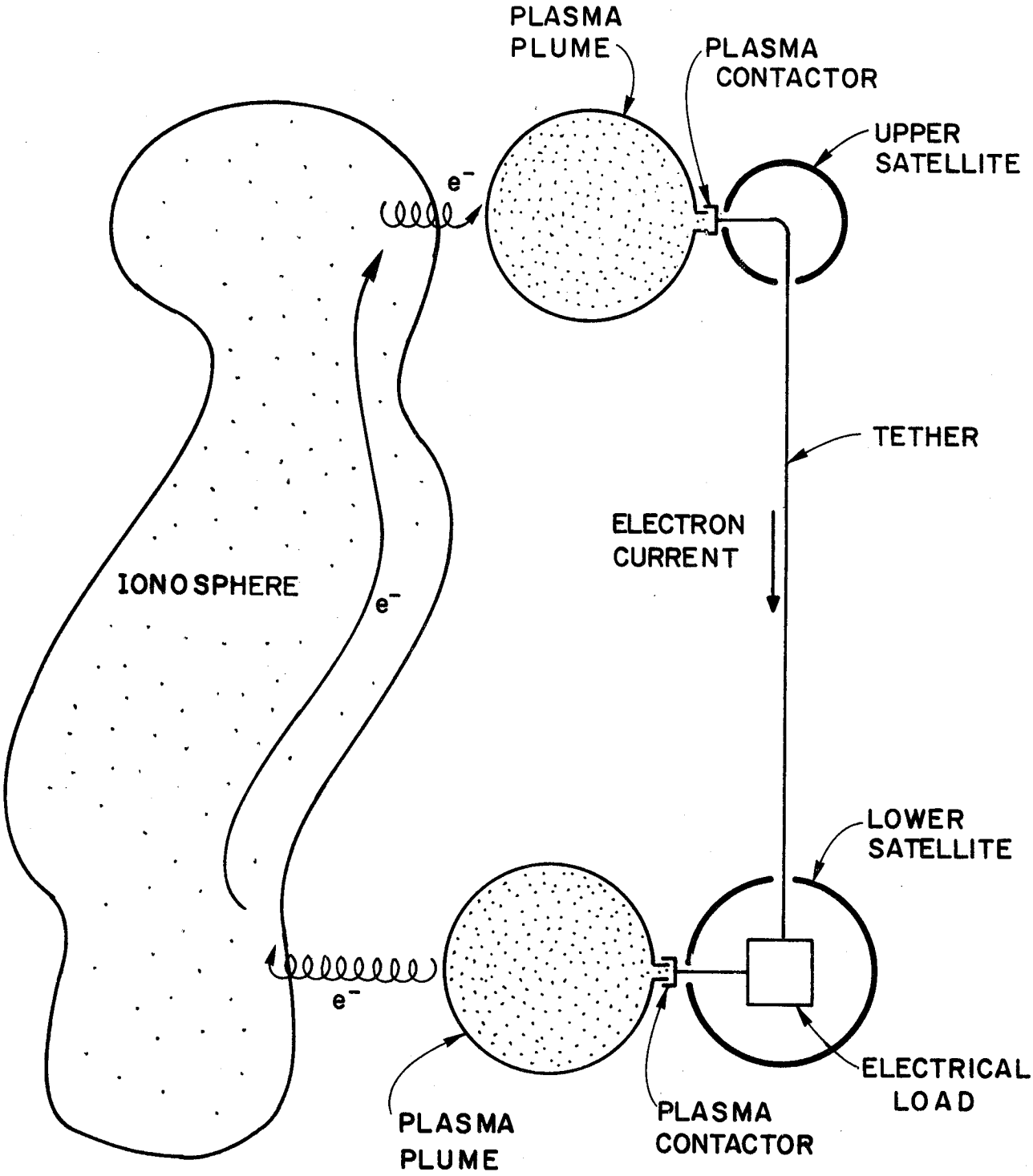

Fig. 1 Electrodynamic Tether Circuit

the dominant charge carrier in this situation so the currents associated with their motion should be addressed. Electron emission would have to be accomplished at the lower satellite shown in Fig. 1 by a device able to produce either electrons or a plasma from which electrons could be extracted. While electron collection, occurring at the upper satellite in Fig. 1, could be accomplished by exposing either a large metal surface or a plasma plume like the one suggested in Fig. 1 to the ionosphere, preliminary research has suggested that the plume generating device would be preferred. This device would generate a plasma plume having a sufficiently large surface area so that it could establish a low impedance plasma bridge to the ambient space plasma that would conduct the tether current.

Appendix A identifies the desirable characteristics of a plasma contactor and suggests preference for a plasma plume-producing device. A simple model of the plasma contacting process, that is detailed in Appendix B, is used to identify both important parameters associated with the process and desirable characteristics of the plasma source used to generate the high density plume. On the basis of this work a hollow cathode discharge is suggested as a plasma source that is well suited to the plasma contacting function. Appendix A also outlines the essential features of the hollow cathode and presents a theory[2] that explains some of its operating characteristics.

The purpose of this report is to describe the operating characteristics of several hollow cathode-based contactors. Much of the effort is focused on evaluation of contactors developed at Johnson Space Center (JSC) for use on the Hitchhiker G[2] and Plasma Motor Generator/Proof of Function[3] experiments. In addition a ring cusp ion source, which was developed, is described and its performance as a contactor is compared to that of a con-

ventional hollow cathode.

EXPERIMENTAL APPARATUS AND PROCEDURE

The apparatus shown schematically in Fig. 2 was constructed to investigate the current/voltage characteristics of plasma contactors. It consists basically of a plasma simulator and the plasma contactor to be tested separated by 2.7 m and contained within a 1.2 m dia. by 5.3 m long stainless steel vacuum tank. Various hollow cathode-based contactors were studied so the one indicated in Fig. 2 should be considered representative of many contactors but the simulator shown was generally the same hollow cathode device. Also shown in Fig. 2 are the meters used to measure currents and voltages together with electrical power supplies needed to sustain operation of the contactor and simulator and to bias the contactor relative to the simulator generated plasma. The symbols designating measured voltages and currents are indicated with the circles representing the meters. The simulator anode is connected to the vacuum tank to provide a return current path between the simulator and contactor in such a way that substantial currents will not flow between the tank wall and the simulated space plasma. These currents are small because the simulated plasma exists at a potential near simulator anode potential so the tank connected in this way is not biased to collect either simulator ions or electrons.

Emissive and Langmuir probes that can be swept through the region between the contactor and simulator, although not shown in Fig. 2, are available to measure plasma properties as a function of position. The simulator plasma source used in the tests, a simple hollow cathode, differs from the one shown in Fig. 3a only in that it utilizes a flat plate anode, 2 cm in diameter and 0.5 mm thick positioned 1 mm downstream of the orifice plate. This simulator cathode utilizes a rolled tantalum foil insert

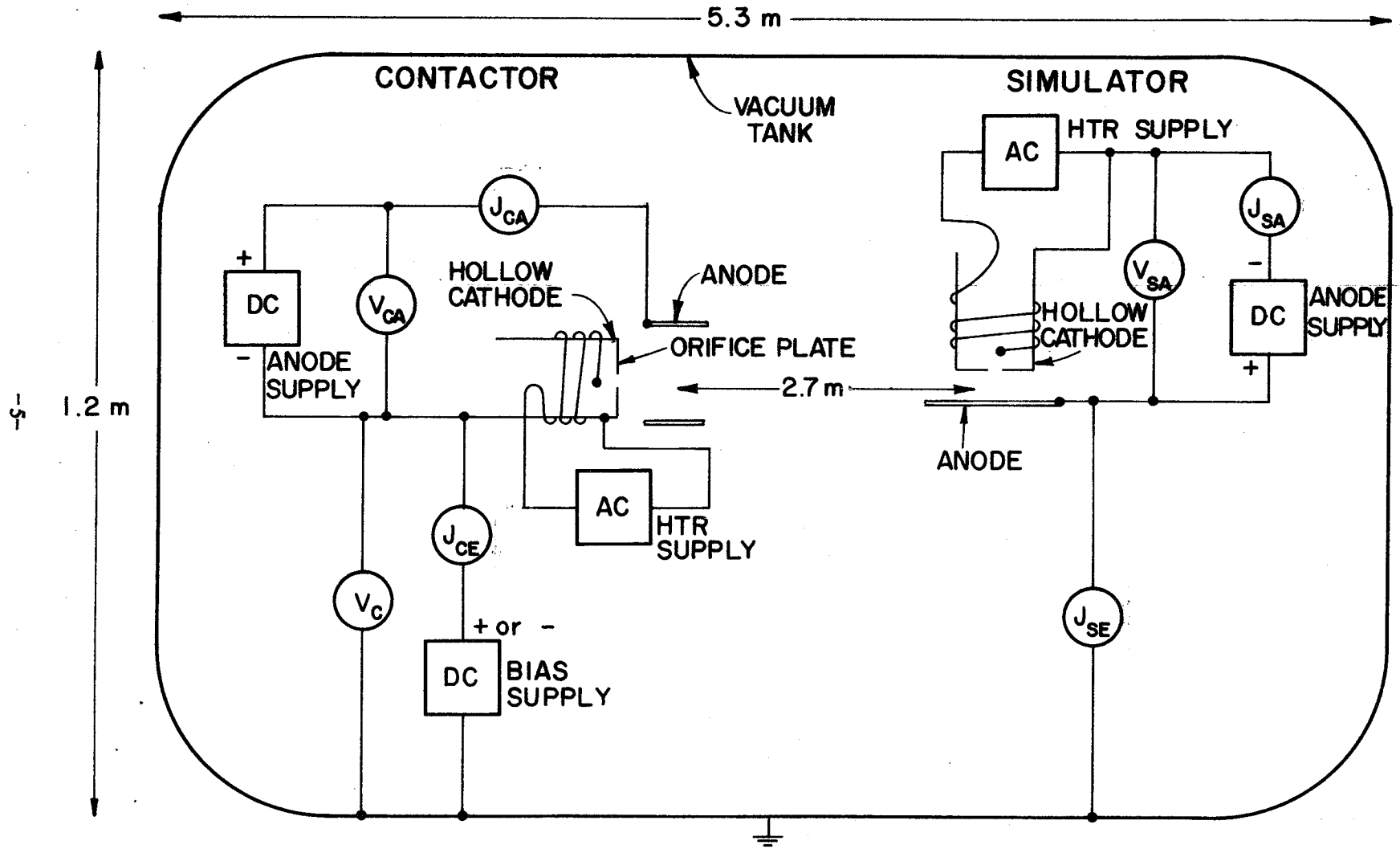

Fig. 2 Schematic Diagram of Test Apparatus

treated with triple carbonate (Chemical R-500) emissive mix to lower its work function. For all tests described here the simulator hollow cathode operation was sustained with a 1.4 sccm xenon flowrate ($\dot{m}_s$) and an anode current J_{SA} of 0.3 A which typically resulted in an anode voltage V_{SA} of about 12 volts. This simulator discharge produced a plasma with a density of the order of 10^6 cm^{-3} midway between the contactor and the simulator.

When a contactor is tested it is generally operated at some time with the simulator off. While operating at a given expellant flowrate and a discharge power established by the anode power supply the contactor is biased from about -50v to +100v relative to the metal vacuum tank using the bias power supply. Biased negative, the contactor will emit electrons to the tank walls and biased positive these electrons will be repelled from the tank so the ions produced downstream of the hollow cathode orifice can be drawn to the tank and measured. As the contactor cathode is biased beyond about 30 volts positive of the tank the ion current drawn to the tank becomes relatively constant at what might be designated the extractable ion current or ion production rate associated with this particular operating condition.

In order to test the current conduction characteristics between the contactor and a simulated space plasma, the simulator discharge must be started and stabilized to provide a stable low density ambient plasma. The ability of the contactor to couple to this simulated space plasma was measured by biasing the contactor over a coupling voltage (V_C) range that was limited by either a) the power supply range (-200v to +200v), b) the occurrence of a contactor electron emission current of 1000 mA or c) the onset of arcing to vacuum chamber walls that suggested these walls were perturbing the test results to the point where the simulation was no longer

valid. Tests were conducted using argon and xenon expellants in contactors operated over a range of contactor anode currents and voltages (J_{CA} and V_{CA}). At each operating point the currents and voltages identified by the symbols in Fig. 2 were measured. The coupling voltage (V_C), contactor emission current (J_{CE}) and simulator emission current (J_{SE}) were the measurements of principal interest. Vacuum tank pressures measured during testing ranged from 3×10^{-6} Torr at low flowrates to 1×10^{-5} Torr at high flowrates.

A number of contactor configurations were investigated during the grant period. These included the simple hollow cathode configuration shown in Fig. 3a, the two extended anode configurations supplied by JSC and shown in Fig. 3b and the ring cusp contactor (a hollow cathode-based plasma source) shown in Fig. 4. The extended anode configurations differ from the conventional configuration in that the separation distance between the cathode and anode is increased from 1 mm to 10 mm and the flat plate anode extends to a 5 cm diameter and has a 13 mm diameter hole while the anode for the conventional cathode is smaller. It was anticipated that the anode extension would facilitate the confinement of the neutral gases escaping from the hollow cathode orifice thereby facilitating higher ion production rates than those of the conventional cathode. Two of the extended anode contactors (007B and 008B) had no heater insulation and had 0.38 mm dia. orifices while the high current contactor had a larger orifice (0.76 mm) and utilized a ceramic heater insulation.

In order to improve the ion production capability beyond that expected with the extended anode contactors, the ring cusp contactor shown in Fig. 4 was designed, built and tested. A key element of this plasma contactor is the hollow cathode shown at the left of this cross-sectional view.

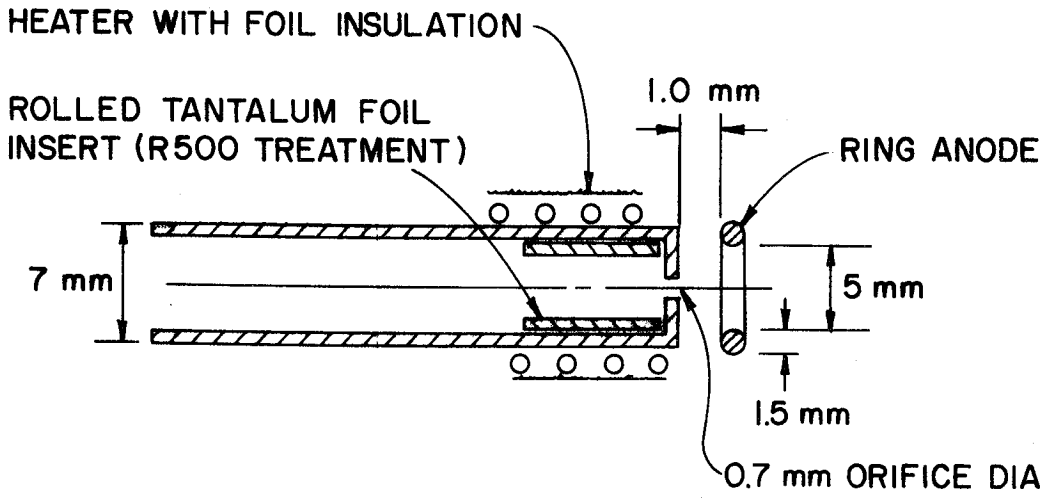

a) CONVENTIONAL CONFIGURATION

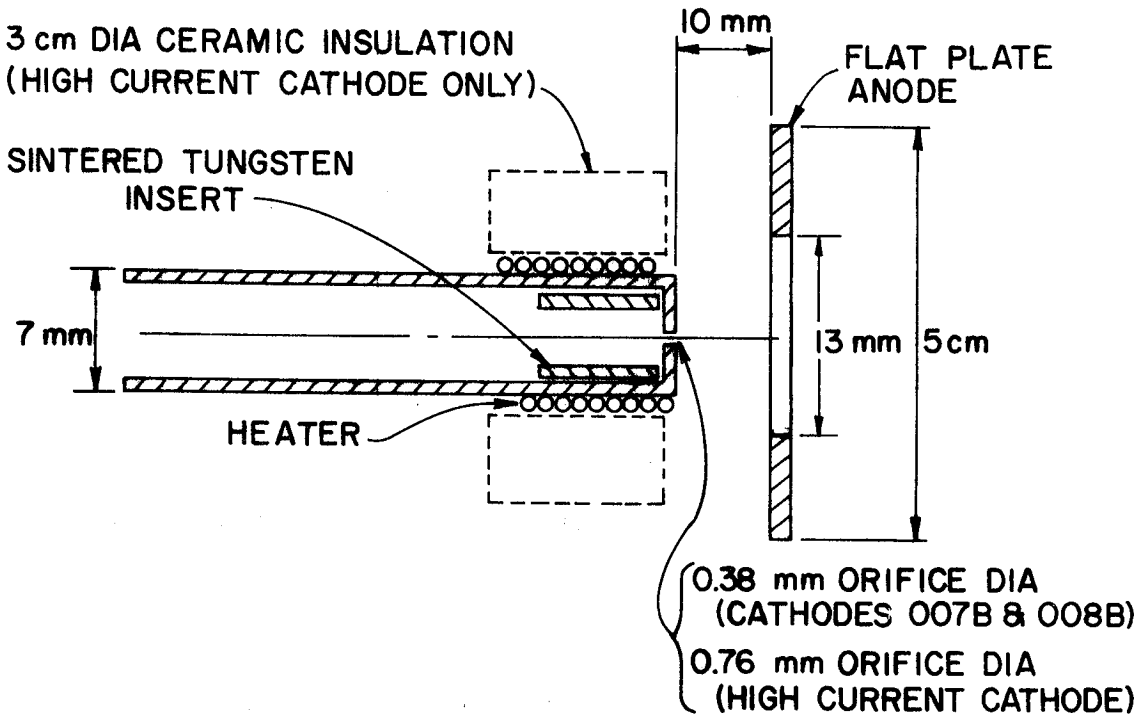

b) EXTENDED ANODE CONFIGURATION

Fig. 3 Hollow Cathode Contactors

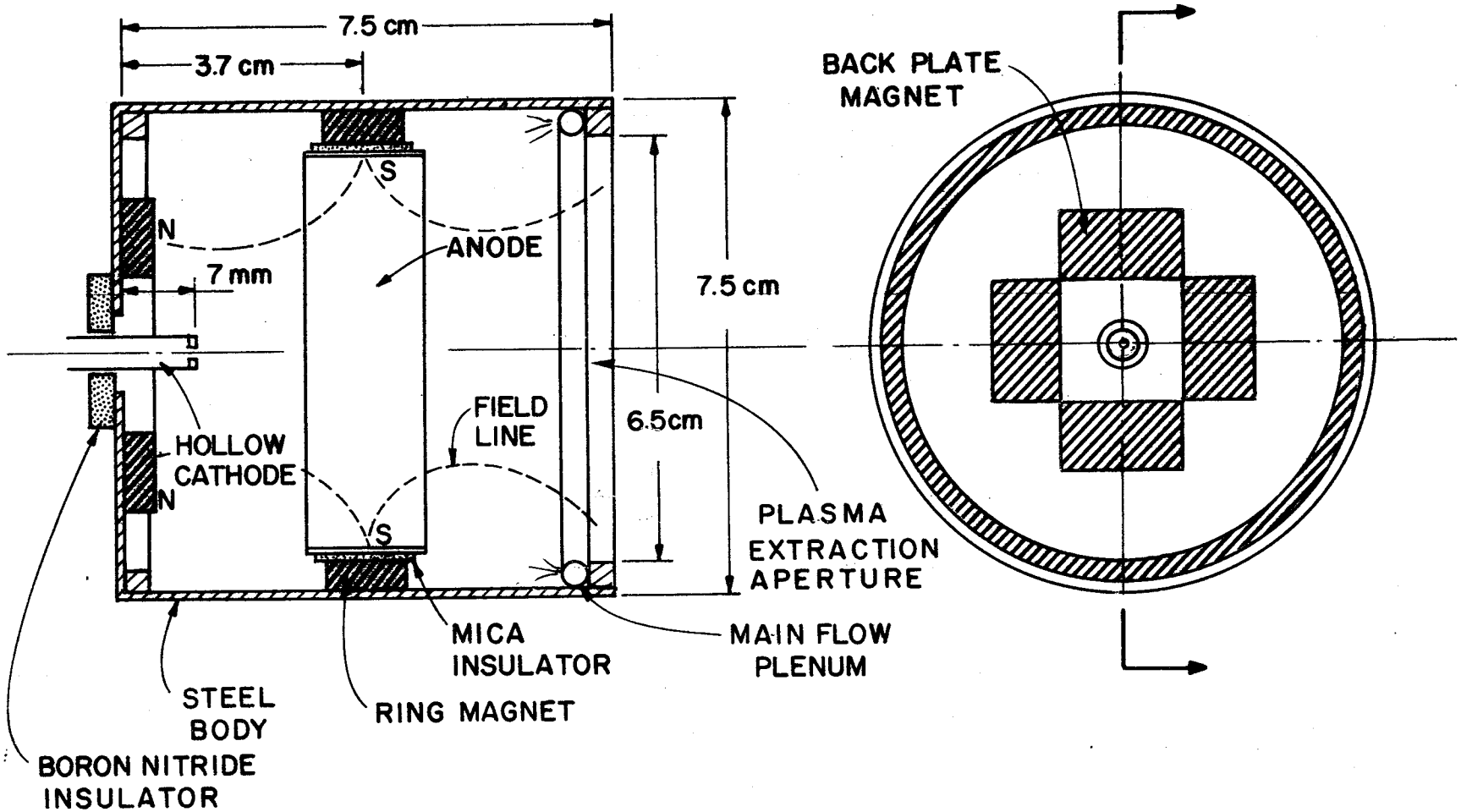

Fig. 4 Ring Cusp Magnetic Field Contactor

It provides electrons directly for the electron emission mode of operation and it supplies electrons to ionize neutral gas and produce ions in the electron collection operating mode. Enhanced ion production is facilitated in both modes of operation by a magnetic field produced within the device. The magnetic field is generated by the magnets shown on the upstream face of the body and in the form of a ring located near the middle of the side wall. These magnets together with the steel body produce a single cusp magnetic field having the shape suggested by the dotted lines in Fig. 4 and shown in more detail by the iron filings map in Fig. 5. Samarium cobalt magnets having a flux density of 0.27 Tesla at their surfaces produce this magnetic field which enhances ion production by containing electrons emitted from the hollow cathode until after they have experienced ionizing collisions. By restraining electron losses to chamber walls the magnetic field also restrains ions produced in the discharge so few reach chamber walls where they would recombine to form atoms. By reducing ion losses to the walls the fraction of the ions produced that are extracted into the plasma plume is increased and the performance of the contactor is enhanced.

The anode in the ring cusp contactor is located adjacent to but electrically isolated from the ring magnet as suggested in Fig. 4. It is because the anode is protected by a magnetic field that energetic electrons drawn from the hollow cathode tend to be confined until they have experienced inelastic collisions some of which produce ions and all of which degrade the energetic electrons' kinetic energy. Because the anode collects low energy electrons in preference to high energy ones in this configuration the contactor power efficiency related to ion production would be expected to be higher than that associated with either conventional or extended anode hollow cathode contactors.

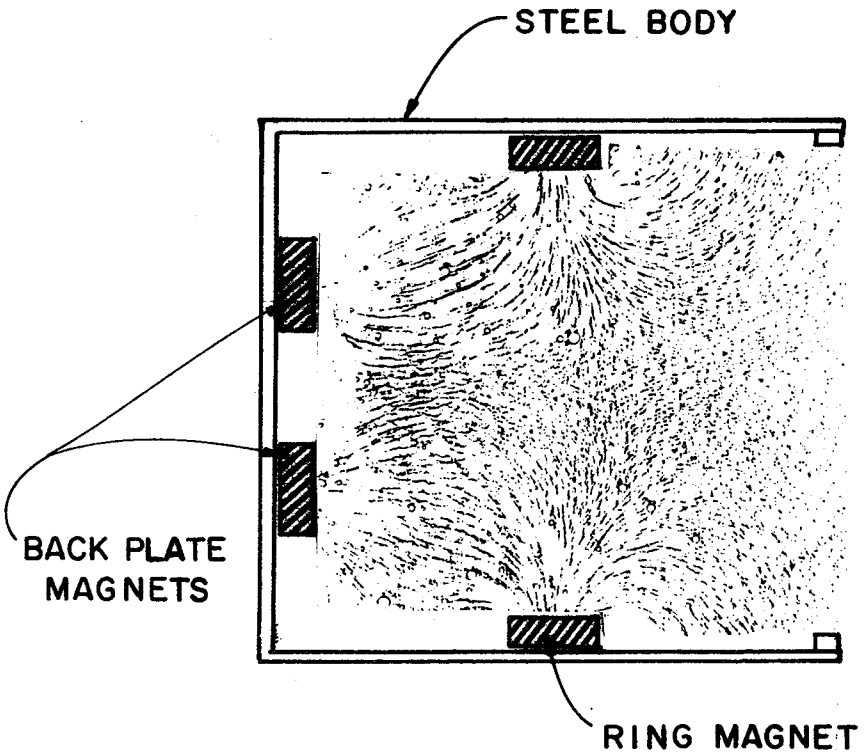

Fig. 5 Magnetic Field Map for 7 cm dia. Ring Cusp Contactor

The ring cusp plasma contactor is also designed so that expellant can be fed through both the hollow cathode and the main flow plenum shown in Fig. 4. The main flow plenum is designed so that atoms are injected into the chamber in the direction opposite to the direction of ion extraction and this enhances the probability for neutral atom ionization before the neutral atoms escape through the plasma extraction aperture. It is noted that the ring cusp ion source is basically the same as a discharge chamber for an ion thruster;[5] it differs only in the device does not include extraction grids. It is also noted that operation of the device requires the same number of power supplies as the conventional or extended anode hollow cathode contactors, namely an anode supply to sustain operation and a heater supply to faciliate startup.

RESULTS

Test results obtained fall into two general categories, one concerned with characterization of the extended anode plasma contactor and the other associated with a comparison between the conventional hollow cathode and the ring cusp plasma contactor. Test results obtained here on the extended anode contactor will eventually be compared with those obtained in space tests. Taken together these tests should provide the key to understanding the plasma contacting process and developing models to describe it.

A number of contactor characteristic curves were obtained during the grant period, and they generally exhibited features illustrated by the generic curves shown in Fig. 6. When the contactors are biased relative to the conducting vacuum tank wall and the plasma simulator is off, the characteristic curves have the general shape of the solid curve. As this curve shows, biasing the contactor negative of the tank causes substantial electron emission from it and biasing it positive of the tank wall induces

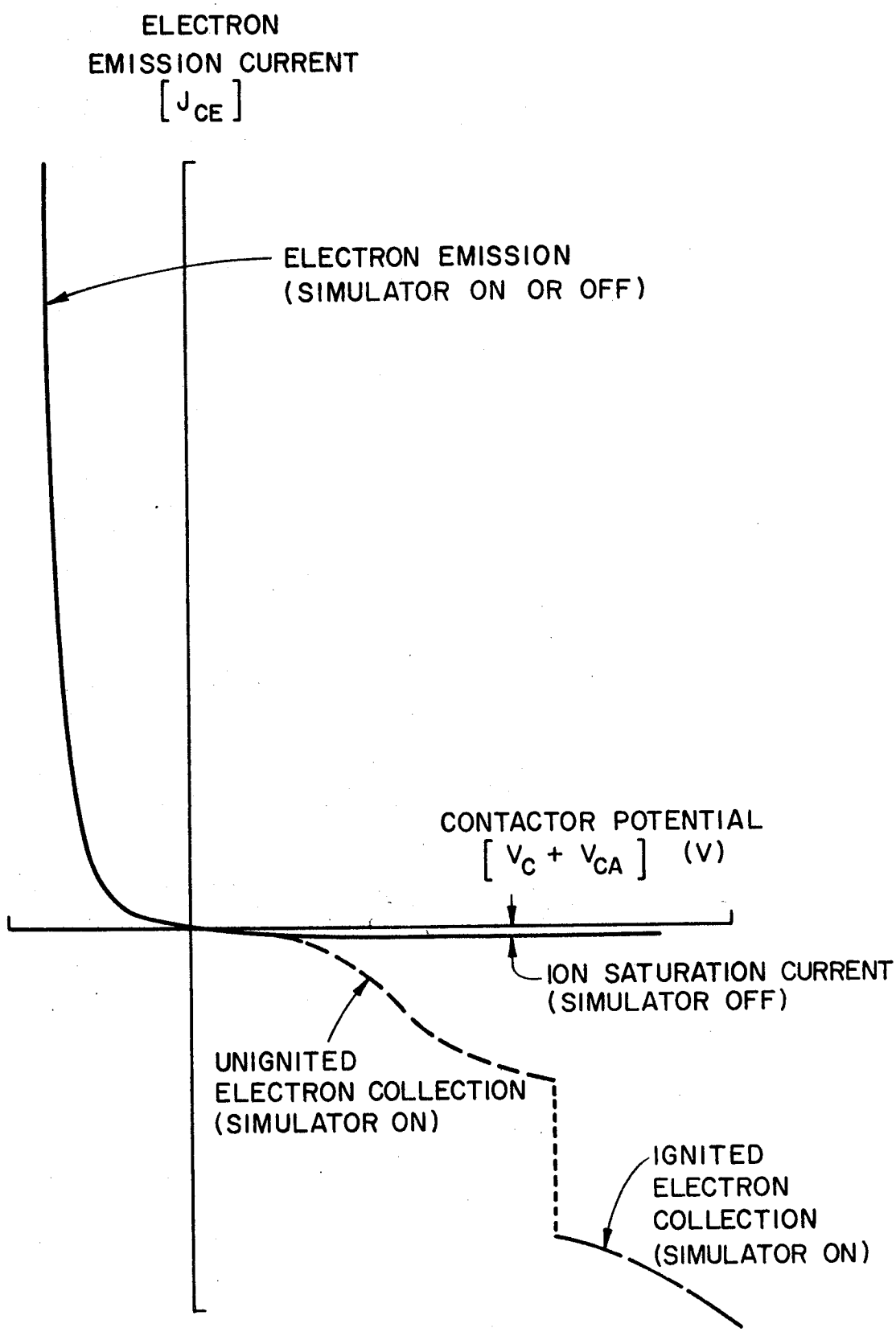

Fig. 6 Generic Contactor Characteristics

a very small ion emission current to flow. The curve shows this diode behavior because the electrons, which conduct the electron emission current, have a mass that is small compared to the ion mass and it is the ions which must conduct the ion emission current i.e. the negative current associated with the solid line. At contactor potentials above about a few tens of volts the ion current saturates at a value assumed to be determined by the rate at which ions were being produced in the discharge. The ion production rate of a contactor measured as this ion saturation current will be used as a measure of the maximum electron current that might be collected on the basis that the electron current collected is proportional to the ion current emitted at the space-charge limited condition. Tests suggest that ion production current depends on the expellant flowrate and discharge power and may range from a fraction of a milliamp to several tens of milliamps. For all of the contactors electron emission currents were quite similar and they exceeded ampere levels as contactor potentials were decreased to values near -40v.

A characteristic curve having the features of the dashed-line in Fig. 6 was typically measured with the simulator turned on. The curve shows that biasing the contactor negative to effect electron emission produces a curve that is essentially the same as the one observed without the simulator operating. This indicates that ions from the simulator do not contribute to any reduction in the space-charge limitation on electron flow from the contactor. This in turn suggests that the electron emission process depends only on electron space-charge effects or that the contactor may not be operating at a space-charge limited condition.

For the case of electron collection and ion emission, the curves with and without the simulator operating depart from each other substantially.

The difference develops because the substantial current drawn from the simulated plasma when it is being generated is not available when the simulator is off. It should be noted that contactor potentials of substantially greater magnitude are required to drive a given electron collection current than are required to drive a similar electron emission current. At low positive contactor potentials Fig. 6 suggests the contactor is unignited i.e. electrons being drawn from the simulated plasma do not induce ionization in the double sheath and/or the high density plume regions of the discharge. In this operating regime the slope of the dotted curve decreases then goes through an inflection point as it increases toward zero slope. The current and voltage at which the inflection point occurs are determined by the contactor design, its expellant flowrate and its discharge power level. The influence of these parameters on the unignited electron collection characteristic curve shape is a major focus of this study. This focus has evolved because electron emission portions of the curves are always quite similar and it is therefore the ability of the contactor to collect electrons from a space plasma that is of primary interest. It should be noted that contactor potential as measured in these experiments and plotted in curves like the dotted one in Fig. 6 is the contactor anode potential measured relative to the tank wall rather than simulated space plasma potential in the tank. Detailed plasma potential measurements[8] have shown that the true potential drop from the contactor anode to the simulated space plasma potential in the electron collection mode is about two-thirds of the contactor potential plotted in figures like Fig. 6. When the contactor is emitting electrons these same studies suggest the contactor anode potential generally remains within a few volts of the simulated space plasma potential. These observations suggest that the voltage

range through which a contactor mustbe varied to achieve current conduction between given electron emission and collection levels will be substantially less than the contactor voltage range determined from figures like Fig. 6.

When contactors are biased sufficiently positive (typically at contactor potentials ranging between 40 and 100 v) they generally undergo transition into the ignited mode of operation suggested by the dashed curve in Fig. 6. Appearance of a visible plume wherein expellant excitation and presumably ionization is occurring accompanies this transition. In the case of the extended anode hollow cathode contactors this plume extended radially outward several centimeters from the region between the cathode and anode. In the cases of the other contactors it extended several centimeters downstream of the anode and appeared spherical in shape. Figure 7 shows actual data describing a typical transition to the ignited mode observed on the high current contactor (Fig. 3b). An important point to note about the data is that the electron current collected by the contactor (circular data symbols) agrees with the electron current emitted by the simulator (square data symbols) in the unignited region but these currents begin to disagree as transition to the ignited mode occurs. When electrons being collected by the contactor are not being emitted by the simulator they must be coming from the metal vacuum tank structure. The appearance of arcs, frequently seen at various points on the tank when contactor potentials exceeded about 100 v, also revealed when electrons were being drawn from the tank. Potentials of order 100 v were frequently achieved at about the point where the contactor was undergoing the transition to the ignited mode of operation (as in Fig. 7). When arcing occurred the perturbing effect of the tank was considered excessive and the data were generally considered invalid. Further, the arcing caused so much noise on the

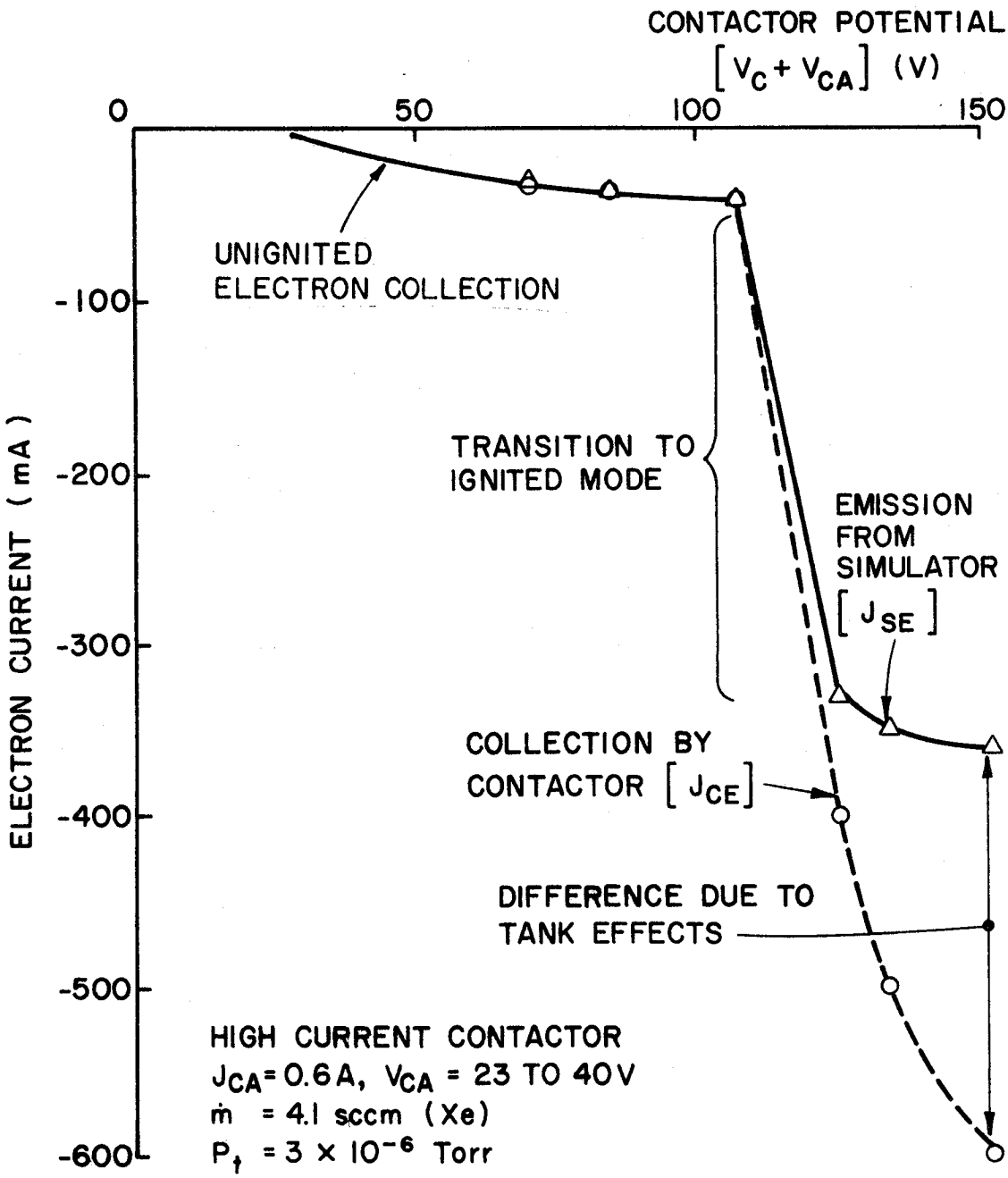

Fig. 7 Experimental Limitations Due to Tank Wall Effects

instrumentation that it was not possible to measure currents and voltages accurately. For this reason data presented herein will concentrate on the unignited mode of electron collection. Data collected under ignited mode conditions will be limited to examples because of the concern about tank effects. Since ignited mode operation results in greater electron collection current levels, however, it is probably the preferred mode of operation and should be investigated further.

A valid simulation of contactor performance in space involves additional requirements beyond the condition that currents not be drawn from the vacuum tank walls, be met. In fact the entire simulation environment should approach that expected in space. This condition would be satisfied if the following variables could be controlled at values as close as possible to those expected in space:

- ambient ionic and neutral gas species and their densities,
- ambient electron density and temperature,
- ambient magnetic field strength.

No attempt has been made in these tests to keep the ionic and neutral gas species at concentrations expected in space. In fact xenon levels in the tank required for contactor operation induce vacuum tank pressures that exceed those in many space environments and one would expect the greater the xenon flowrate and background pressure in the tank the poorer the simulation. Much additional research is considered to be needed before the magnitude of the perturbing effects of the ambient tank gases will be known.

The plasma densities in the dilute, simulated space plasma have also not been measured during all of the tests. In fact the present experimental apparatus is such that the Langmuir probe can only be swept through the

region extending to 1 m downstream of the contactor so it cannot probe the plasma adjacent to the simulator. The plasma in the region downstream of the conventional contactor has been probed at low xenon flowrate levels in a separate study[7]. Typical plasma density profiles measured in these tests are reproduced in Fig. 8. They suggest electron densities ranging from 10^5 - 10^6 cm^{-3} exist in the region intermediate between the contactor and simulator at a low flowrate and that these densities increase with increasing xenon flowrate. These electron densities might also change when the discharge goes into the ignited electron collection mode but this effect has not yet been studied. It has been observed that operation at high neutral density and high electron collection currents causes illumination throughout the entire vacuum tank. This illumination is almost certainly due to atomic excitation and it is also almost certainly accompanied by ionization which would also be expected to increase plasma densities.

In order to investigate the importance of the ambient magnetic field, tests in which the ambient field was varied to determine its effect on contactor performance were conducted under a separate study.[7] These tests indicated that the geomagnetic field penetrates the vacuum tank and is oriented at an angle of ~70° to the line joining the contactor and simulator (i.e. the tank axis). Changes in this magnetic field from about 0.5 gauss to near zero were induced using a Helmholtz coil. No significant change in conventional contactor performance accompanied these changes. For the tests described herein the geomagnetic field was not nulled and a 0.5 gauss field inclined at ~70° to the tank axis existed throughout the plasma interaction region.

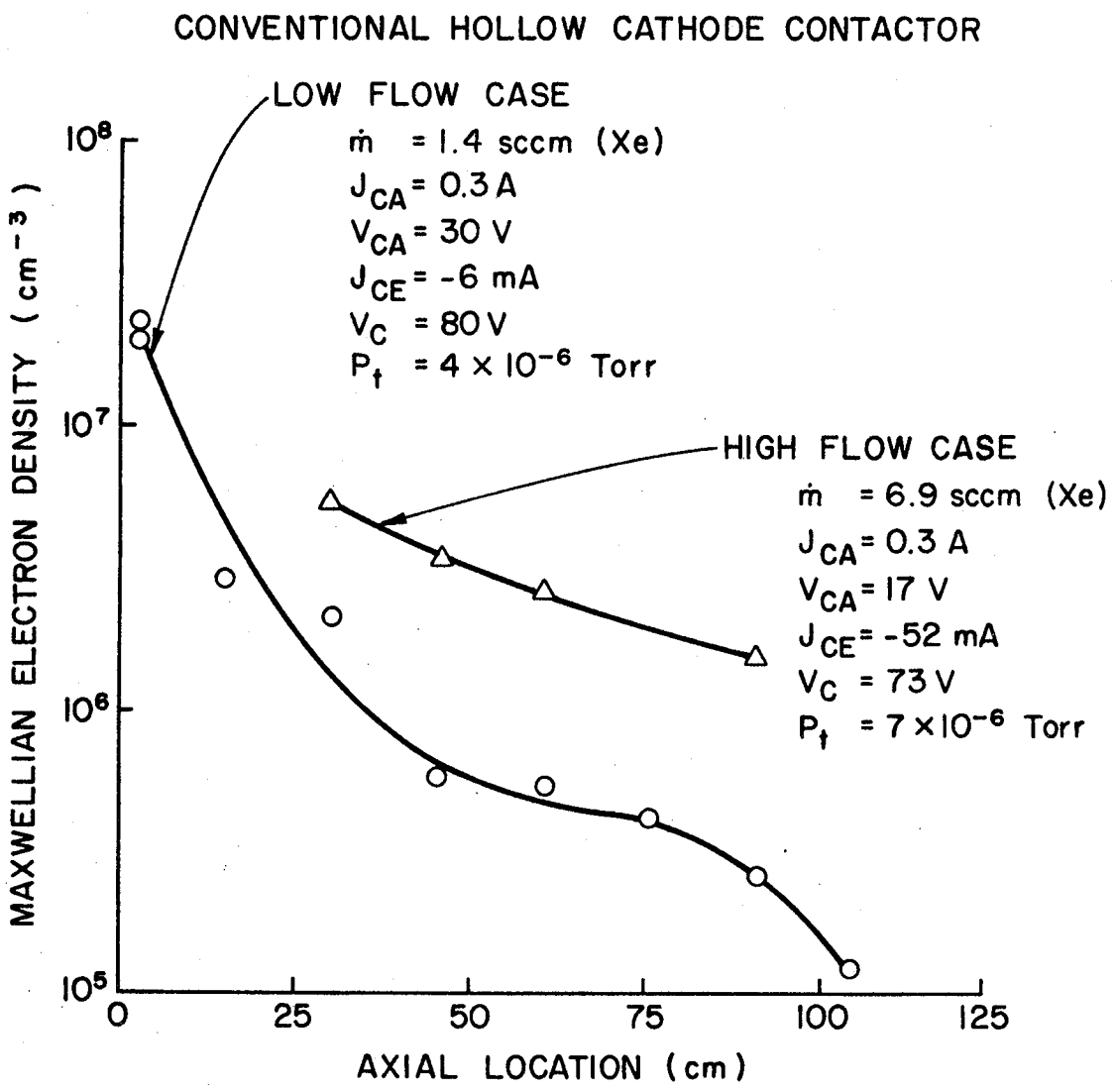

Fig. 8 Plasma Density Profiles

Extended Anode Plasma Contactor Results

Typical curves describing the performance of JSC contactor 007B (the extended anode configuration of Fig. 3b) are shown in Fig. 9. This particular contactor had been operated at JSC until it began to exhibit poor performance and poor restart characteristics. In order to facilitate testing, the contactor was rejuvenated by applying triple carbonate low work function mixture (Chemical R-500) to its sintered tungsten insert and tests were then performed on it. The open circular symbols in Fig. 9 describe the performance measured with a 1.4 sccm xenon flowrate ($\dot{m}$) and 0.6 A anode current (J_{CA}). At these conditions the contactor shows good performance in the electron emission mode but does not exhibit a very high electron collection current even when the contactor potential approaches 150 volts. At a 90 v contactor potential the data show a drop (i.e. increase in the electron current being collected) suggestive of the transition to the ignited mode. When these data were recorded no luminous plume was observed, but intense luminous plumes had not been observed at that time so the discharge was not being scrutinized for such luminosity.

After collection of the data represented by the open circular symbols in Fig. 9, cathode 007B was allowed to operate near zero emission for several minutes and then the contactor was biased and its electron emission/collection curve was remeasured. The data associated with this second collection sequence are shown by the solid circular symbols in Fig. 9. Comparison of these data with the open symbols shows the degree of reproducibility generally achieved from test to test. Increasing the expellant flowrate from 1.4 sccm to 4.1 sccm while maintaining the 0.6 A contactor anode current caused the performance curve to change to the dotted one associated with the square symbols. At this flow some evidence of

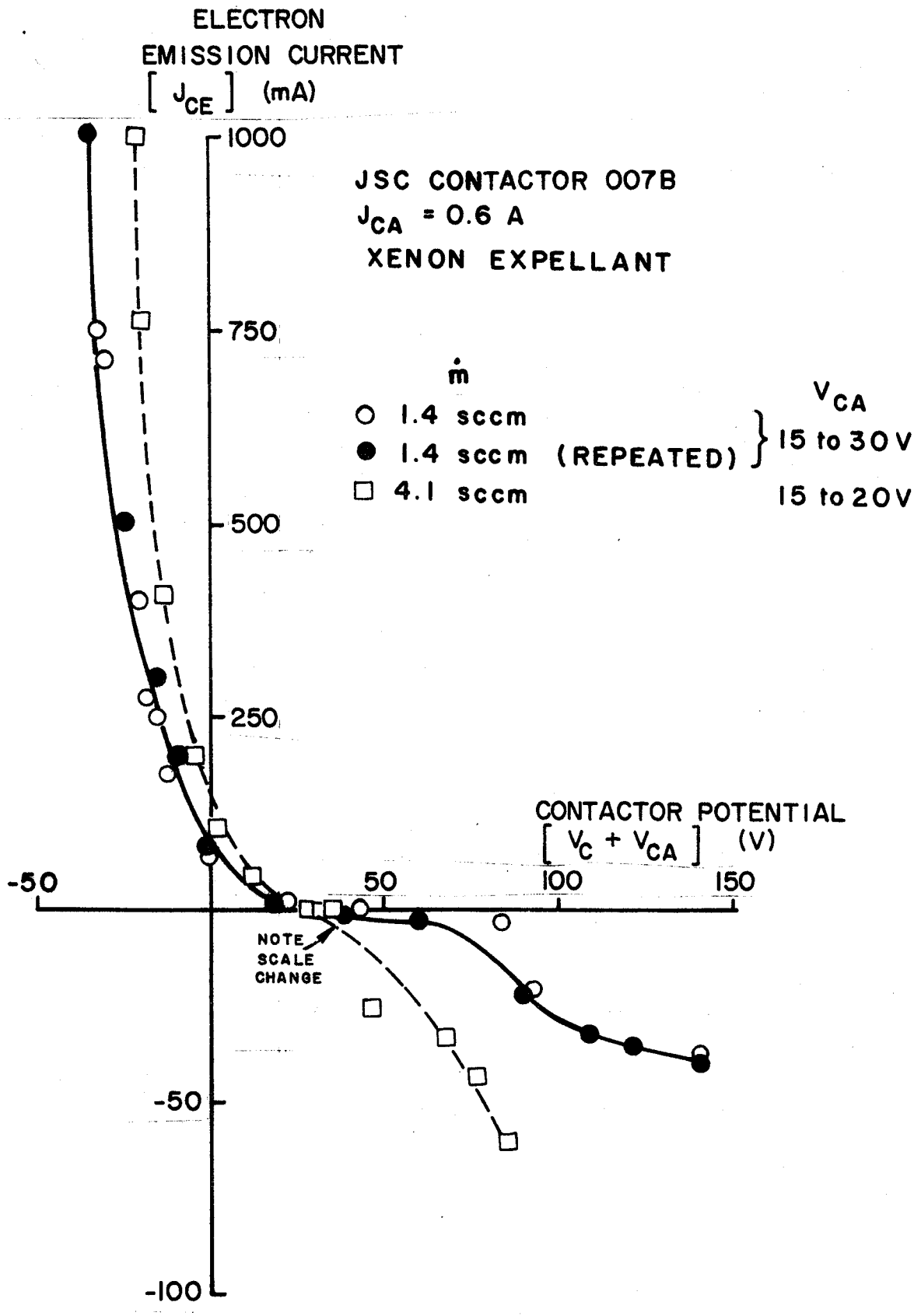

Fig. 9 Contactor 007B Performance at Low Flow and Moderate Anode Current - Xenon

a transition to the ignited mode operation is again apparent; this time at a contactor potential near 40 v. During collection of the data for Fig. 9, the contactor anode voltage varied as the contactor potential was changed. For the lower flowrate case the contactor anode voltage was about 30 volts during electron collection but as the contactor potential was reduced below about -10 volts, the contactor anode potential began to decrease and reached about 15 volts when substantial electron current was being emitted. Anode voltage may decrease because operation at a higher emission current facilitates increased ionization in the region between the anode and cathode orifice and as a result a lower contactor voltage will sustain the contactor anode current. At the higher flowrate this contactor anode voltage change varied through a much smaller range as the data in the legend of Fig. 9 show. Note that the last data point shown for each curve generally represents the last one that could be obtained without inducing the arcing that generally accompanied that transition to ignited mode electron collection at high coupling voltage conditions.

Additional curves describing the behavior of JSC plasma contactor 007B and the effect of xenon flowrate and discharge power on its performance are given in Figs. 10 to 12. Figure 10, for example, shows that the contactor anode potential remains constant at about 10 volts when the expellant flowrate is increased through the range from 6.9 to 27 sccm. The electron emission and electron collection portions of the performance curves describing these contactors are improved as a result of these increases in flowrate. Further, the data at 6.9 sccm were collected both at the beginning and end of the test sequence (approximately 30 minutes between the two tests) and once again the performance data are reproducible.

The data presented in Fig. 11 were all obtained at a relatively high

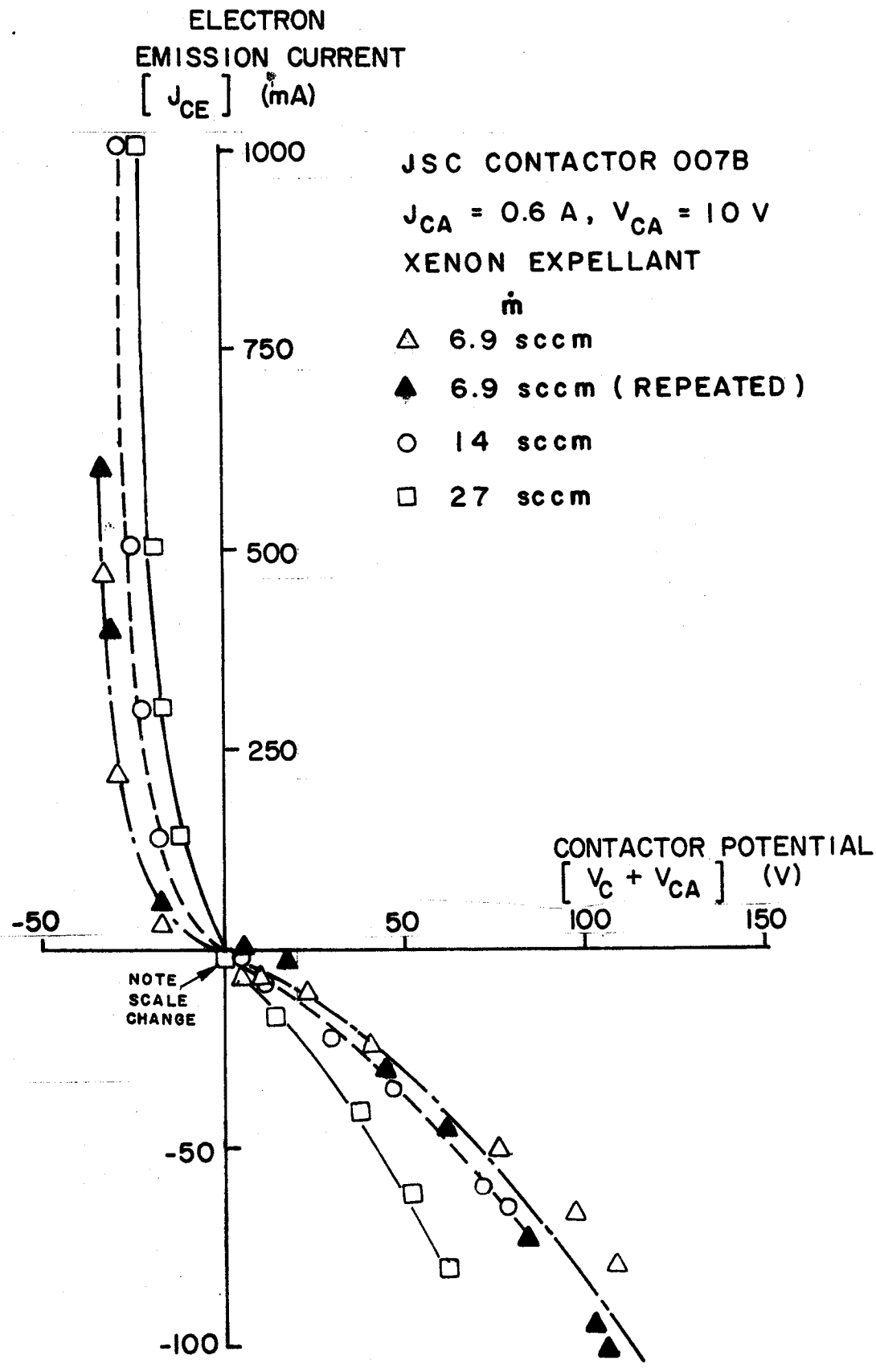

Fig. 10 Contactor 007B Performance at High Flow and Moderate Anode Current - Xenon

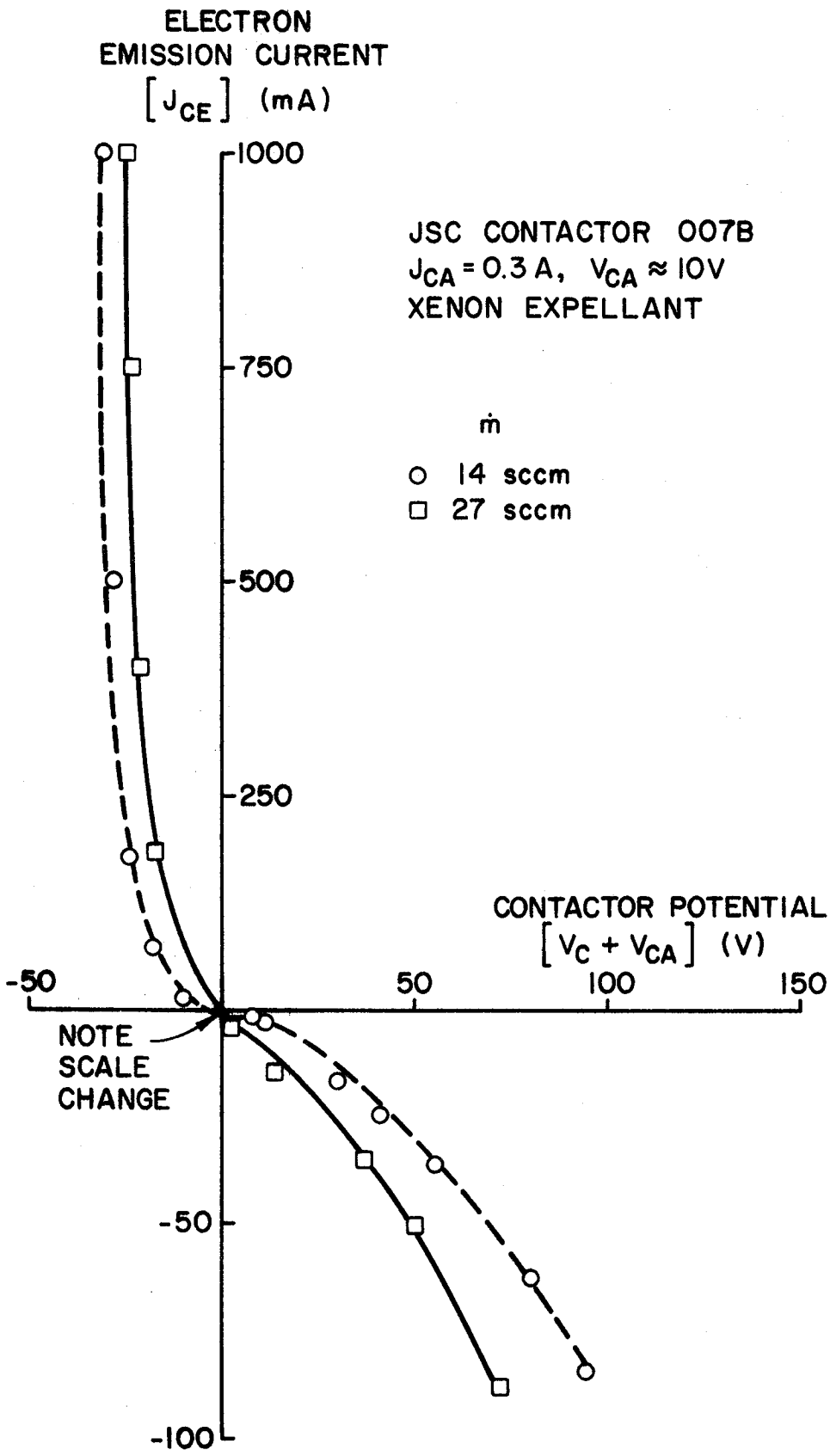

Fig. 11 Contactor 007B Performance at high Flow and Low Anode Current - Xenon

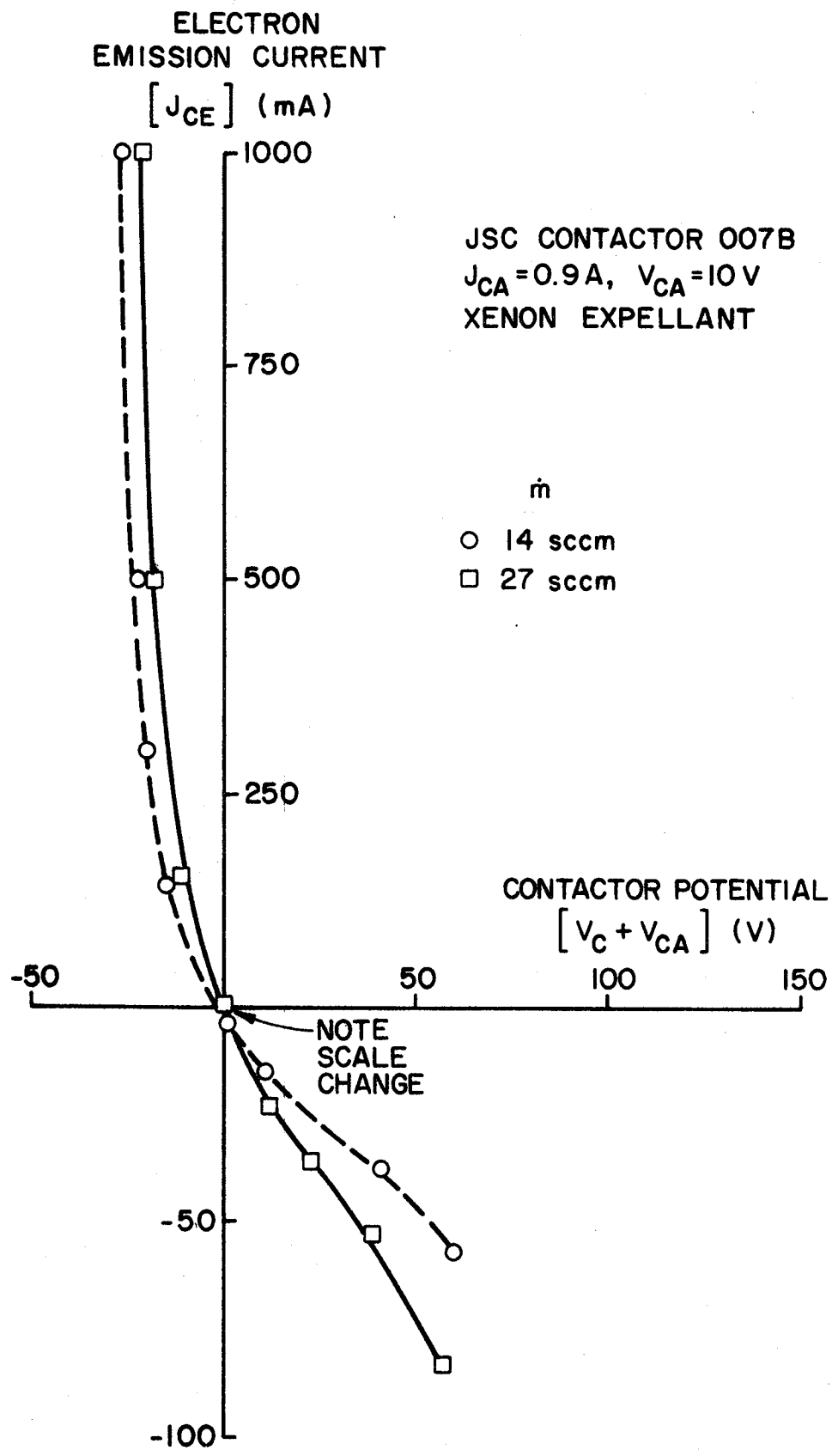

Fig. 12 Contactor 007B Performance at High Flow and High Anode Current - Xenon

flowrate, but in contrast to Fig. 10, they were collected at the lower contactor anode current of 0.3 A. At these high flowrates the data suggest a reduction in contactor anode current to 0.3A does not induce any significant degradation in contactor the performance in either the electron emission or electron collection operating modes. Similarly Fig. 12 shows that increasing the contactor anode current from 0.6 to 0.9 A. does not induce a substantial improvement in contactor performance at these high flowrates in either the electron emission or collection modes of operation.

The curves of Figs. 9 to 12 all suggest that the hollow cathode contactor characteristic approaches that of an ideal contactor. This suggests that the hollow cathode-based devices being investigated have many of the desirable characteristics identified in Appendix B (e.g. high electron production capability, passive emission control and switchover capability).

It has been pointed out in the theoretical model in Appendix B that the maximum (or limiting) electron collection capability of a contactor may be related to its ion emission capability. This should in turn be related to its ion production capability. Figure 13 shows how the ion current extracted from the contactor discharge by biasing the contactor positive with the simulator off varies with contactor discharge power. These data show that increases in discharge power and xenon flowrate (up to 27 sccm) induce increases in the ion production rate of the contactor. The data also show, however, that increasing the xenon flowrate beyond 27 sccm does not result in further increases in the ion production rate. The solid square symbols in Fig. 13 designate performance with the cathode heater power reduced 14% below the operating conditions associated with the open square symbols. While these two sets of data may suggest a slight improvement in ion production capability as heater power is increased, the

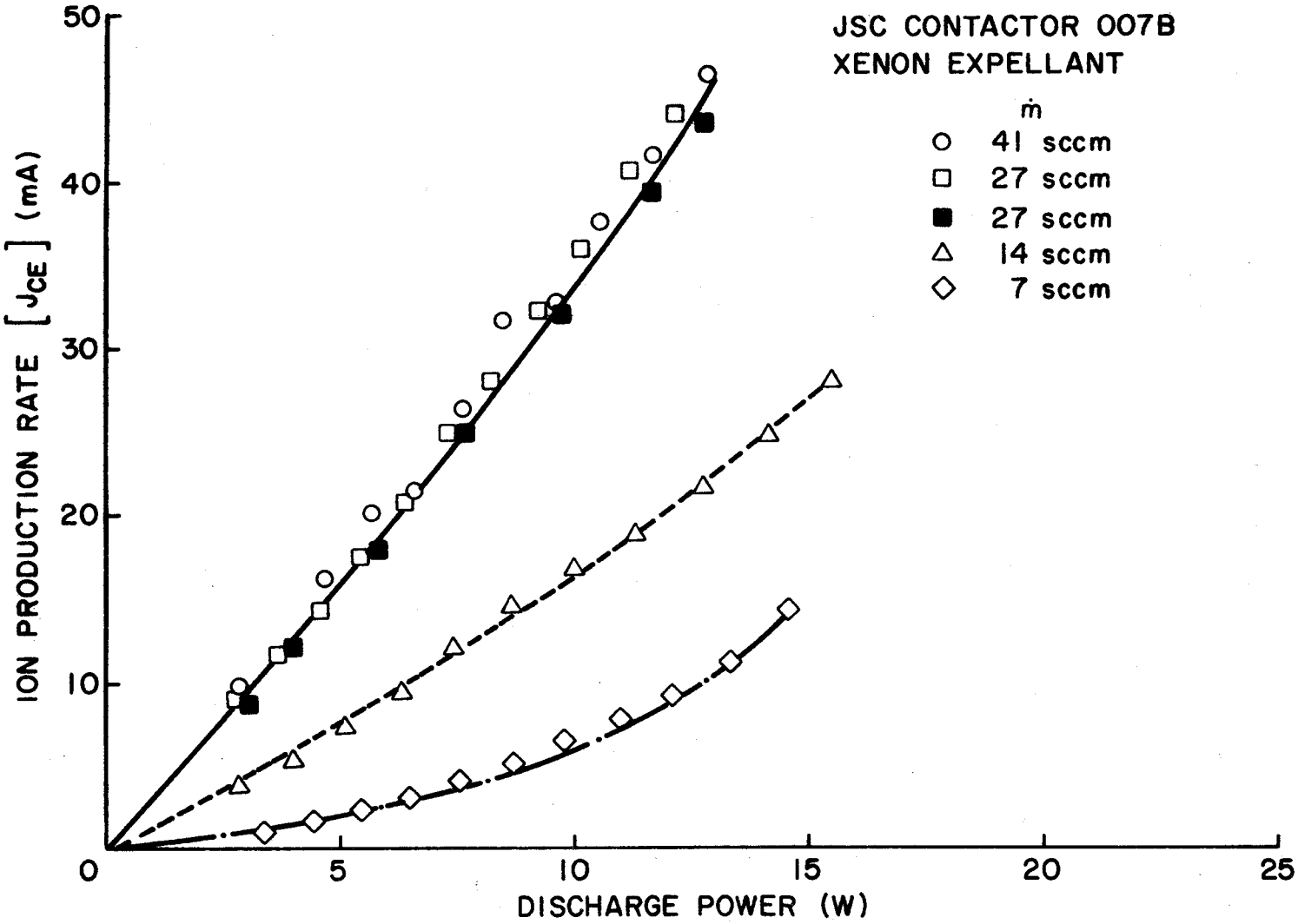

Fig. 13 Effect of Discharge Power and Flow on Ion Production - Xenon

observed change is probably within the limits of experimental error.

Figure 14 shows performance curves at two contactor anode current levels and a moderately high xenon flowrate for the high current version of the extended anode contactor developed at JSC (see Fig. 3b). This contactor was, like contactor 007B, received from JSC with its insert either contaminated or depleted of low emission mix. It was rejuvenated by treating the insert with chemical R-500 so electrons could be drawn from its insert without operating the insert at excessively high temperatures. Comparison of the curves of Fig. 14 with those of Fig. 9 suggests both contactors exhibit similar performance with contactor 007B being slightly better. This suggests the changes in the high current contactor orifice diameter and the heater insulation did not affect performance substantially.

The performance of JSC contactor 007B operating on argon expellant is described in Figs. 15, 16, and 17. Figure 15 shows typical performance curves while Figs. 16 and 17 show the effects of expellant flowrate and discharge power on its ion production capability. Comparison of the data in these figures with data obtained for xenon shown in Figs. 9 through 14 suggests considerably poorer performance is realized when argon is used in place of xenon. Still the data on these figures show the same general trends identified with xenon expellant. Figure 15 again shows that both the electron emission and electron collection performance capability of this contactor improves as flowrate is increased. Figure 16 shows the contactor's ion production capability also improves with flowrate although incremental effects of changes in flowrate differ for the two expellants as comparison of Figs. 13 and 16 shows. This is believed to be related to the lower ionization cross sections at a given energy for argon as compared to xenon.[5]

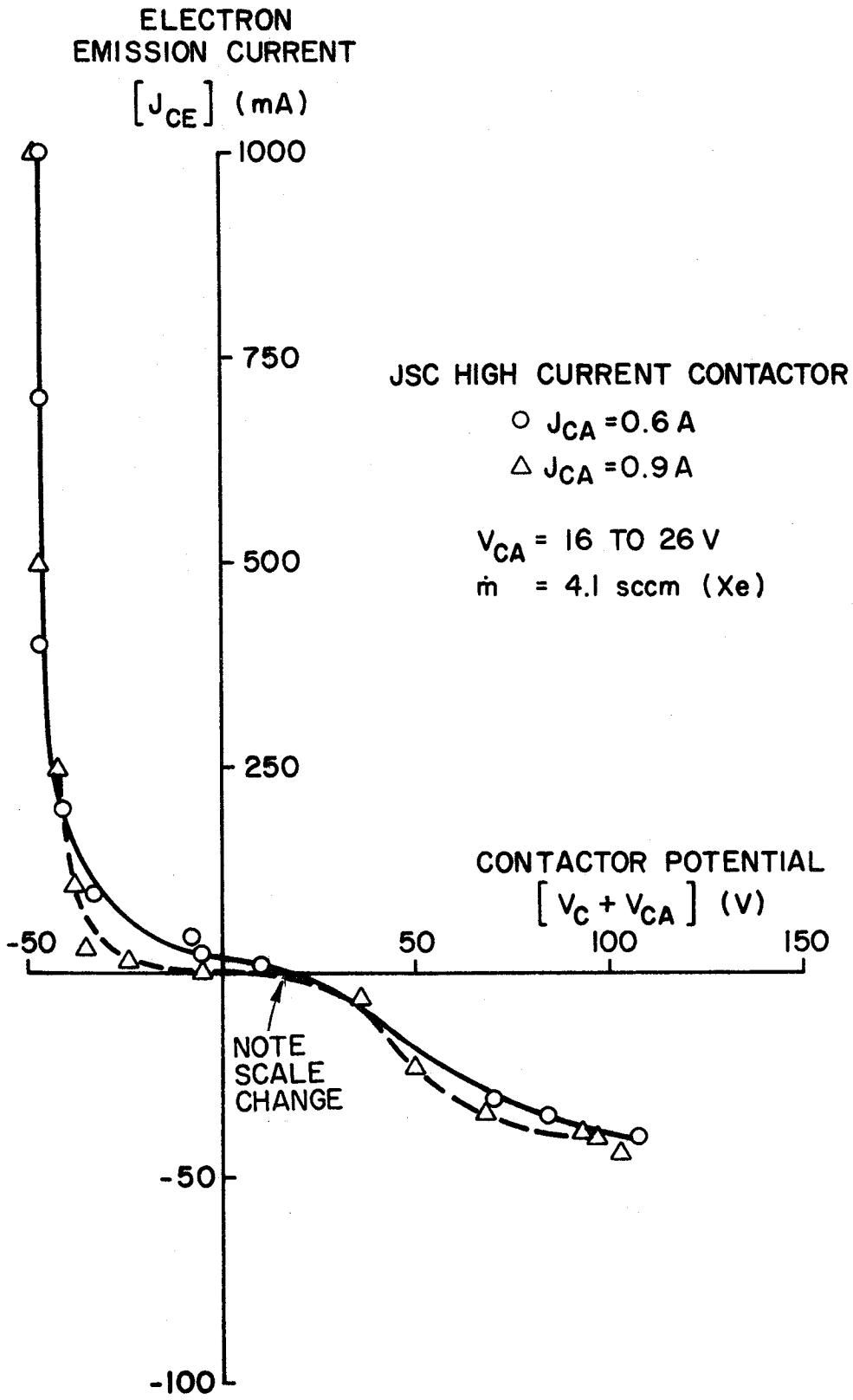

Fig. 14 High Current Contactor Performance at Low Flowrate - Xenon

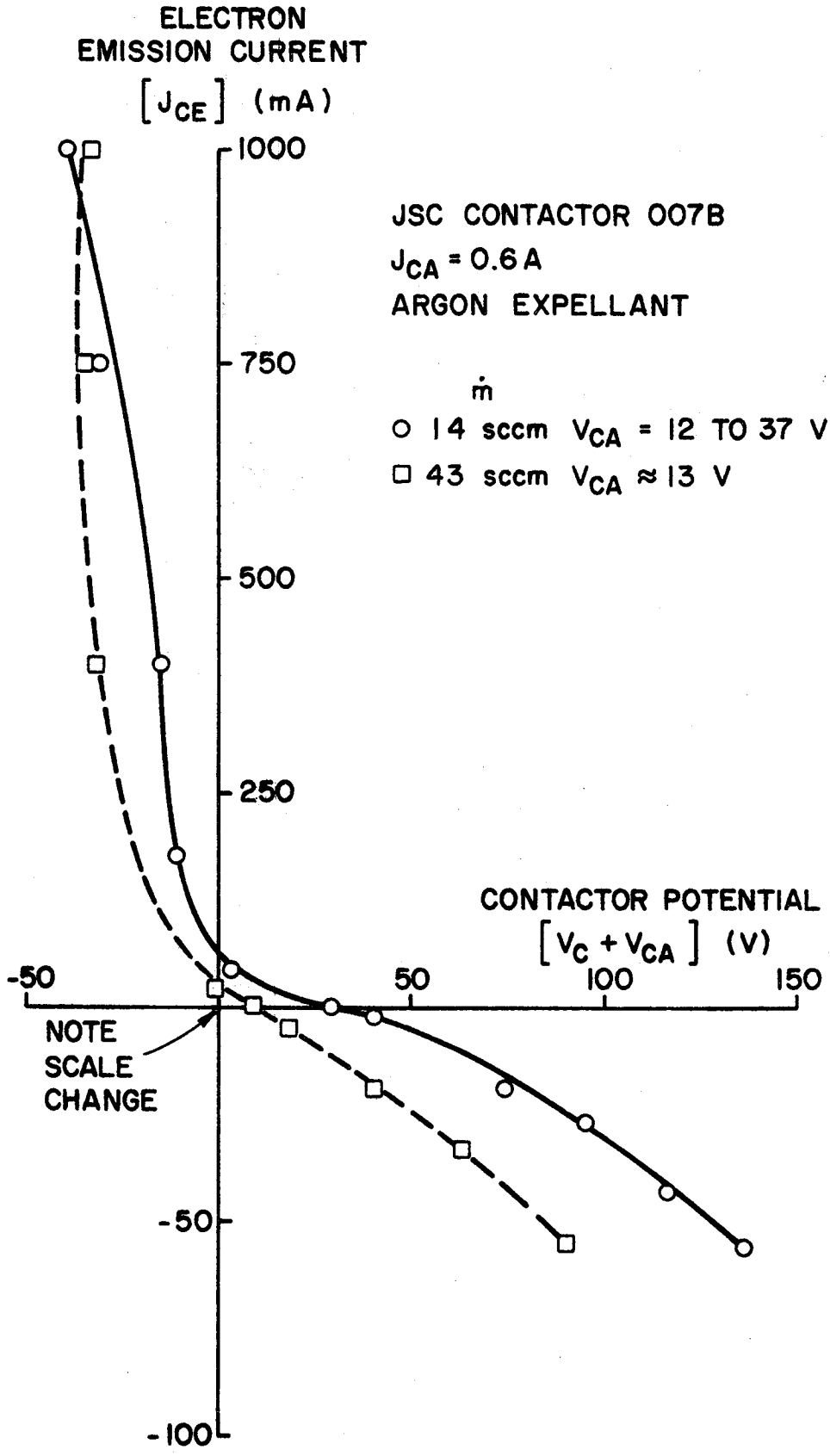

Fig. 15 Contactor 007B Performance Characteristics at High Flowrate and Moderate Power - Argon

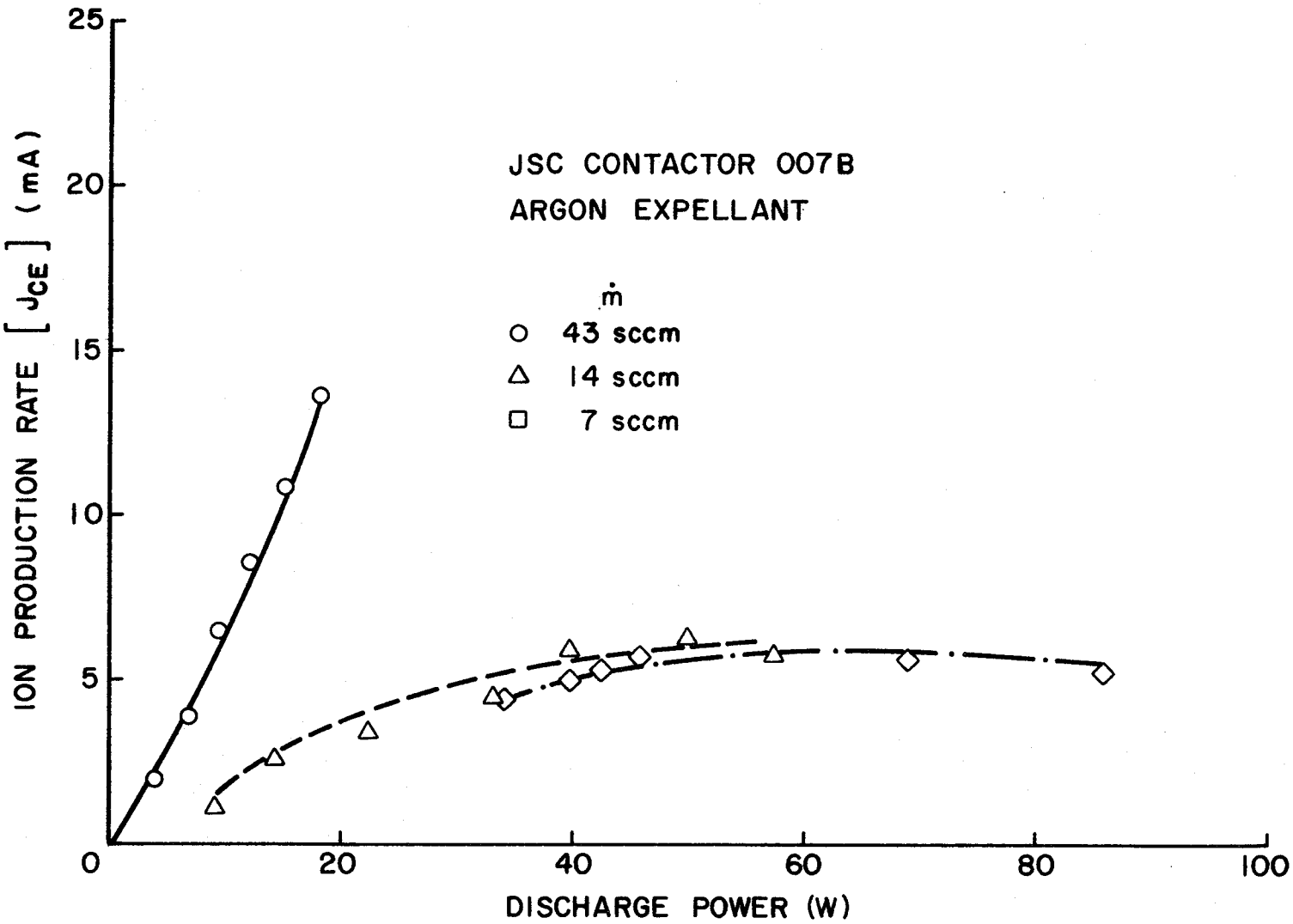

Fig. 16 Effect of Discharge Power and Flow on Ion Production - Argon

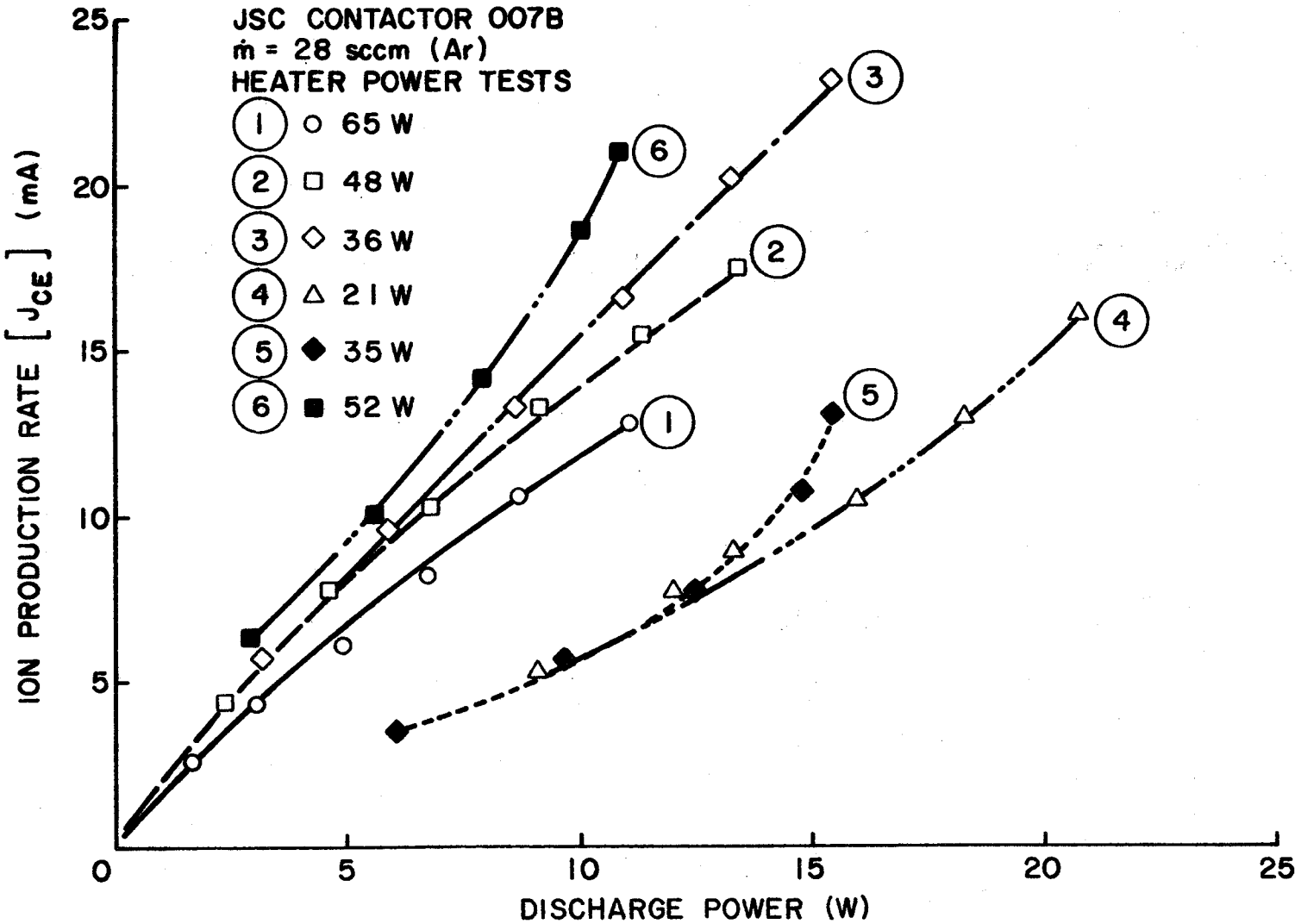

Fig. 17 Effect on Heater Power on Ion Production

In Fig. 17 the effects of cathode heater power on the extractible ion current, i.e. ion production rate, are examined. The test associated with the data presented in this figure began by stabilizing contactor operation at a 65w heater power over a long period of time. This produced the ion production rate curve identified by the number 1. The heater power was then decreased in steps with three minute intervals between these step changes in heater power in a sequence suggested by the numbers associated with each of the curves in Fig. 17. As can be seen from the figure initial decreases in heater power caused the ion production rate curves to shift upward. The decrease in power from 36w to 21w (curves 3 to 4), however, caused a sudden decrease in ion production and it was necessary at this point to increase the heater power to 35 w (curve 5) to keep the contactor operating. After operation for approximately three minutes at the conditions associated with curve 5 an additional increase in heater power to 52 w resulted in the performance suggested by curve 6. It is not understood why the changes in heater power induced the observed changes in the ion production rate of the contactor, however, these changes may have been associated with changes in the emission characteristics of the cathode insert. It is also believed that these changes were transient in nature so a longer period of time between steps may have allowed the insert to stabilize nearer its initial condition and resulted in curves that were considerably closer together. It is also instructive to compare curve 1 of Fig. 17 with corresponding data contained in Fig. 13 (at a flowrate of 27 sccm). This comparison indicates that the ion production rates for a cathode running on argon are significantly poorer than for the same cathode running on xenon.

In Fig. 18a, the contactor ion production rate is examined as a

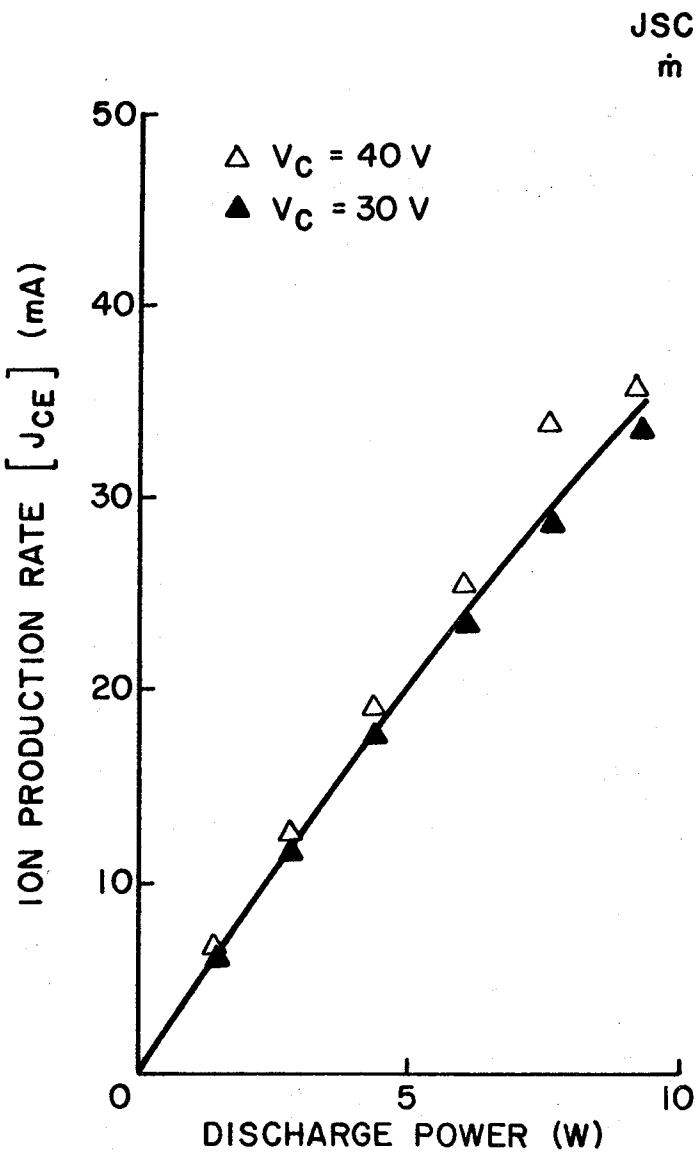

Fig. 18a Effect of Bias Voltage on Ion Extraction

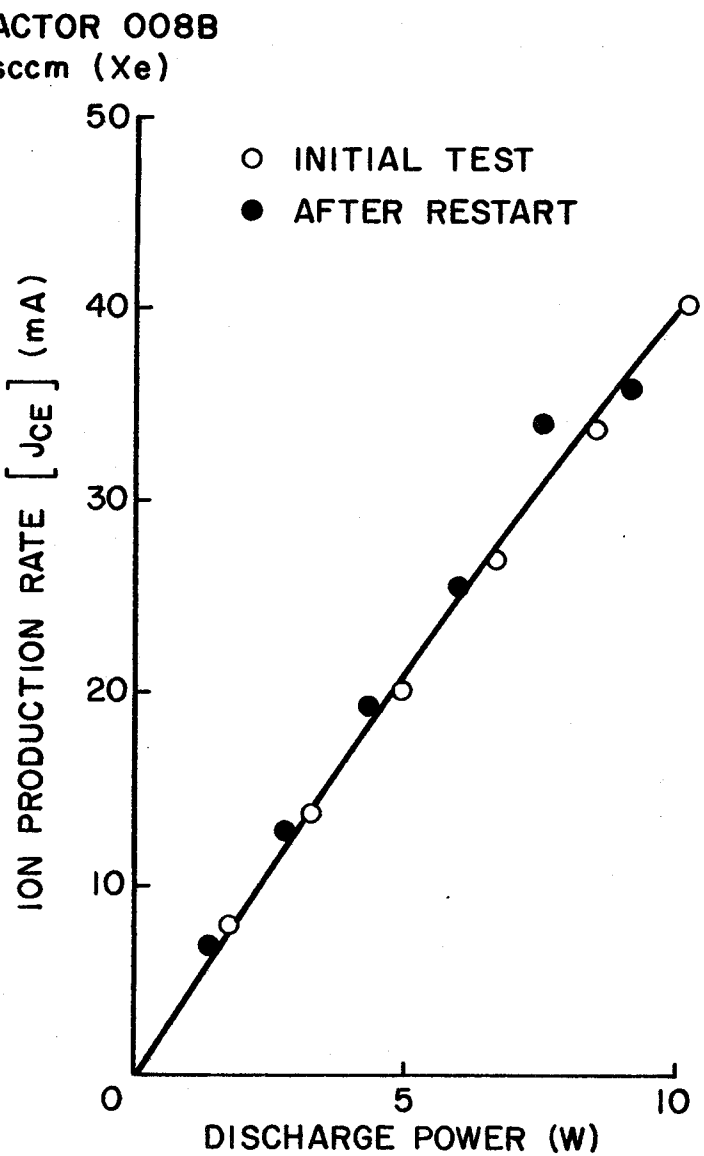

Fig. 18b Repeatability Test

function of discharge power for two cases, one in which the measurement was made with the contactor cathode (V_c) 40 volts positive of the tank and the other with it 30 volts positive of the tank. These data suggest that a 30v bias is sufficient to assure ions are extracted as rapidly as they are produced, i.e. the measurements are made in the ion saturation region of the discharge characteristic. Most tests were actually run with a 40v positive contactor bias but when arcing was observed to occur this was occasionally reduced to 30v. In Fig. 18b the effect of shutting down contactor 008B allowing it to cool for five minutes and then restarting it is shown. The data suggest no change in the ion production current that can be extracted from the cathode as the result of undergoing this cyclic shutdown/restart process.

In order to investigate the performance data comparability for two contactors constructed identically operating on xenon, the data contained in Figs. 19 and 20 (contactor 008B) were collected and compared to the data in Figs. 9 through 14 (contactor 007B). Contactor 008B is identical to 007B except for the fact that contactor 008B was in a virgin, unoperated condition while contactor 007B was rejuvenated after it had been operated at JSC until it became hard to start and began to exhibit a high anode voltage during operation. Typical performance curves measured with contactor 008B are shown in Fig. 19 where the effects of contactor anode current and heater power are also examined at a xenon flowrate of 27 sccm. Comparison of these data with corresponding data in Figs. 10, 11, and 12 suggest that contactor 008B performs substantially the same as contactor 007B. The data of Fig. 19 also suggests that variations in heater power on contactor 008B, measured at the 0.6 A anode current condition, produce no significant change in the electron emission/collection performance curves. This same

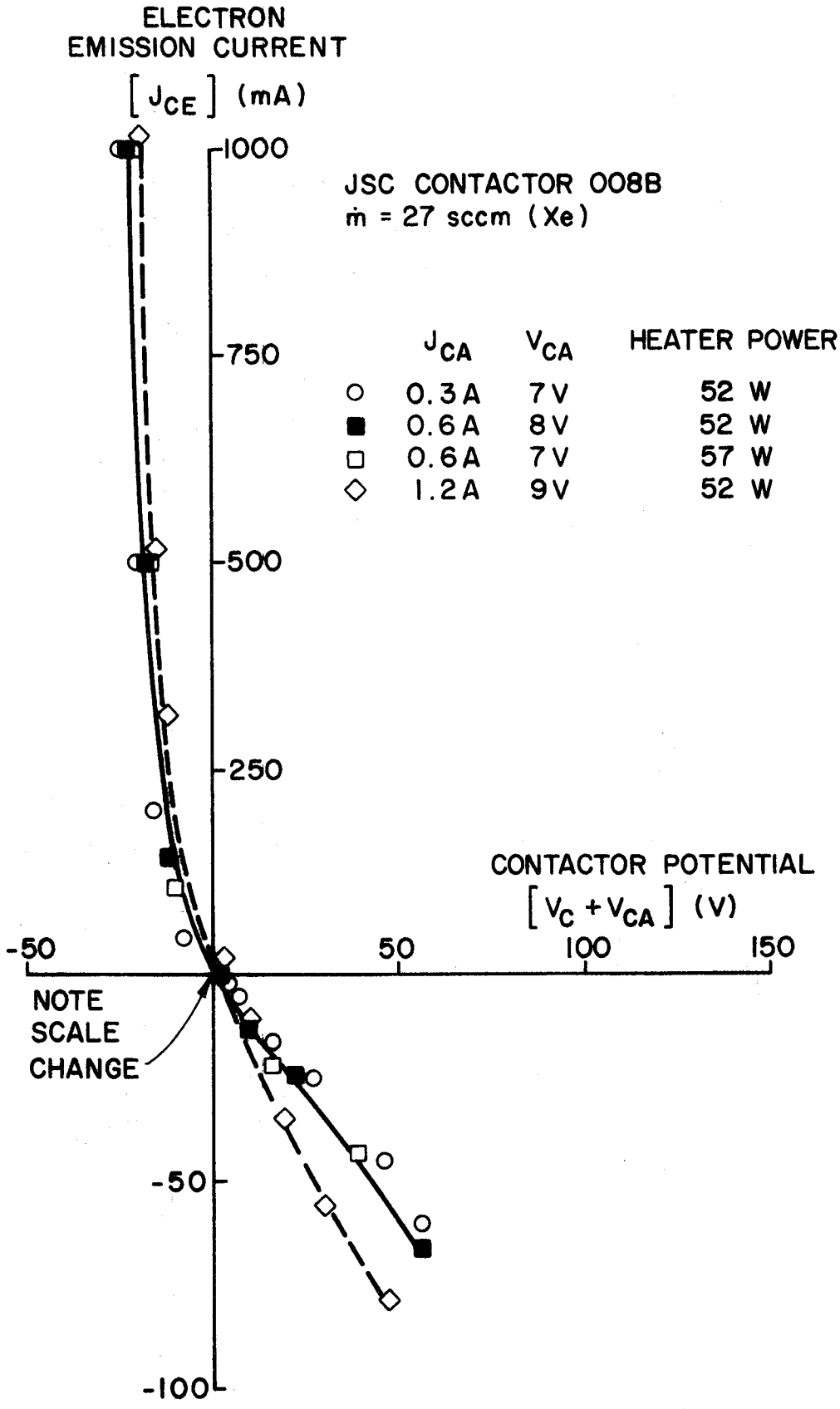

Fig. 19 Contactor 008B Performance at High Flow - Xenon

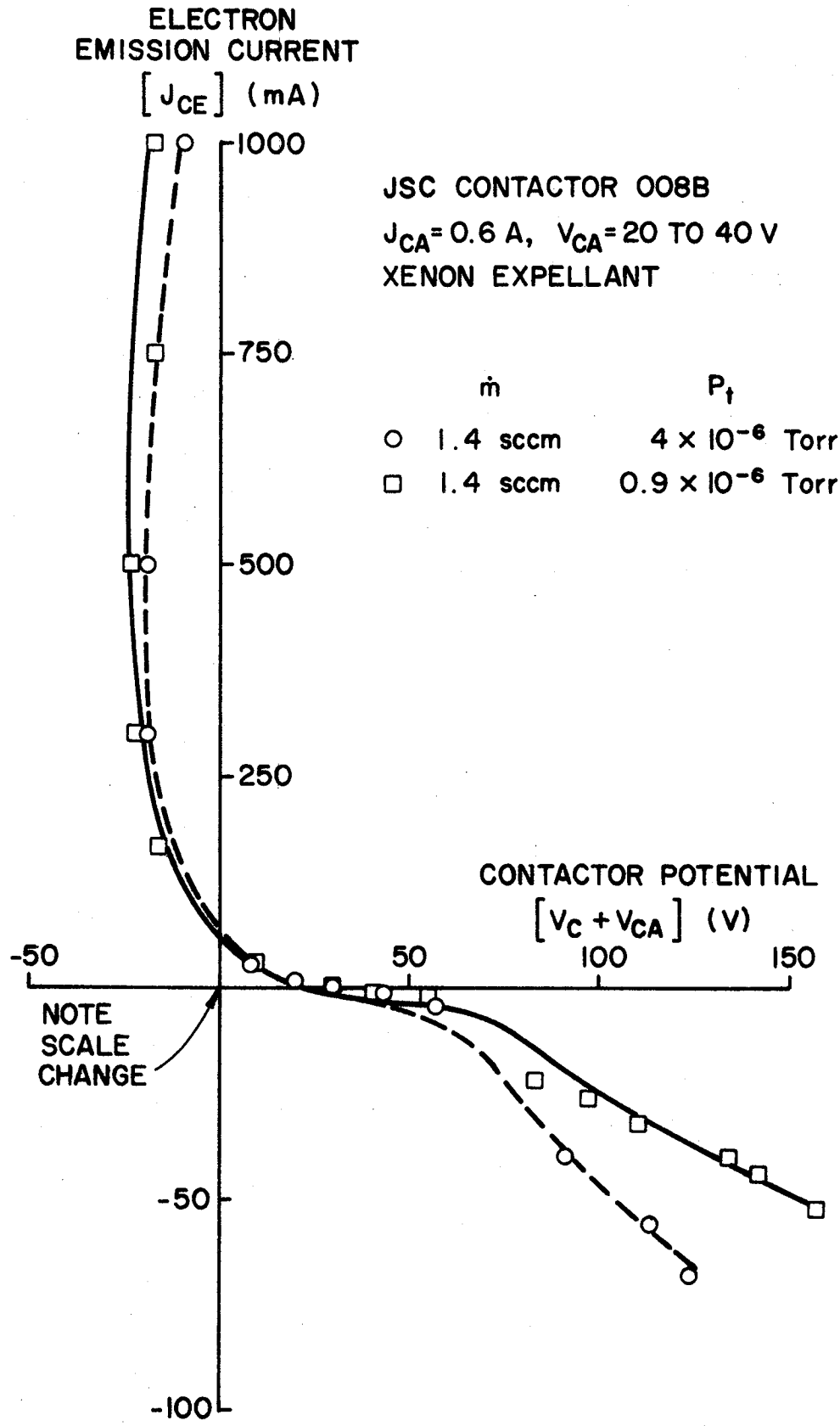

Fig. 20 Contactor 008B Performance Characteristics Showing Effect of Background Pressure

behavior, while not measured on contactor 007B, would be expected to be the same.

In Fig. 21 the effect of varying the background vacuum chamber pressure by bleeding xenon into the tank while holding the expellant flowrate through the cathode orifice constant is examined. These data suggest that increases in background pressure facilitate a modest improvement in performance in the electron emission region and a somewhat greater improvement in the electron collection region. The fact that improved performance occurs in both modes suggests an increase in the ionization rate in the region between the simulator and contactor accompanies tank pressure increases. The rates are believed to be comparatively smaller than rates occurring in ignited electron collection mode operation because the luminous plume under these conditions was less intense than it was in ignited mode operation. Presumably the ions resulting from this ionization induced the improved performance by reducing further the effects of space-charge limitations.

In Fig. 22, the performance of contactor 008B is measured using argon expellant and found to be essentially the same as that of contactor 007B operating on this expellant (compare with Fig. 15). One again observes poorer performance with argon relative to xenon as comparison of Figs. 19 and 22 reveals. Figure 22 also shows a minimal performance improvement accompanis increases in the argon flowrate from 29 sccm to 43 sccm.

In Fig. 23, the effect of varying contactor anode current on the performance of contactor 008B is examined and it is observed that changing this parameter causes no significant changes in the electron emission or electron collection characteristics. Comparison of Figs. 19 and 23 again shows the performance degradation associated with using argon rather than xenon expellant. The rate at which argon ions can be extracted from the

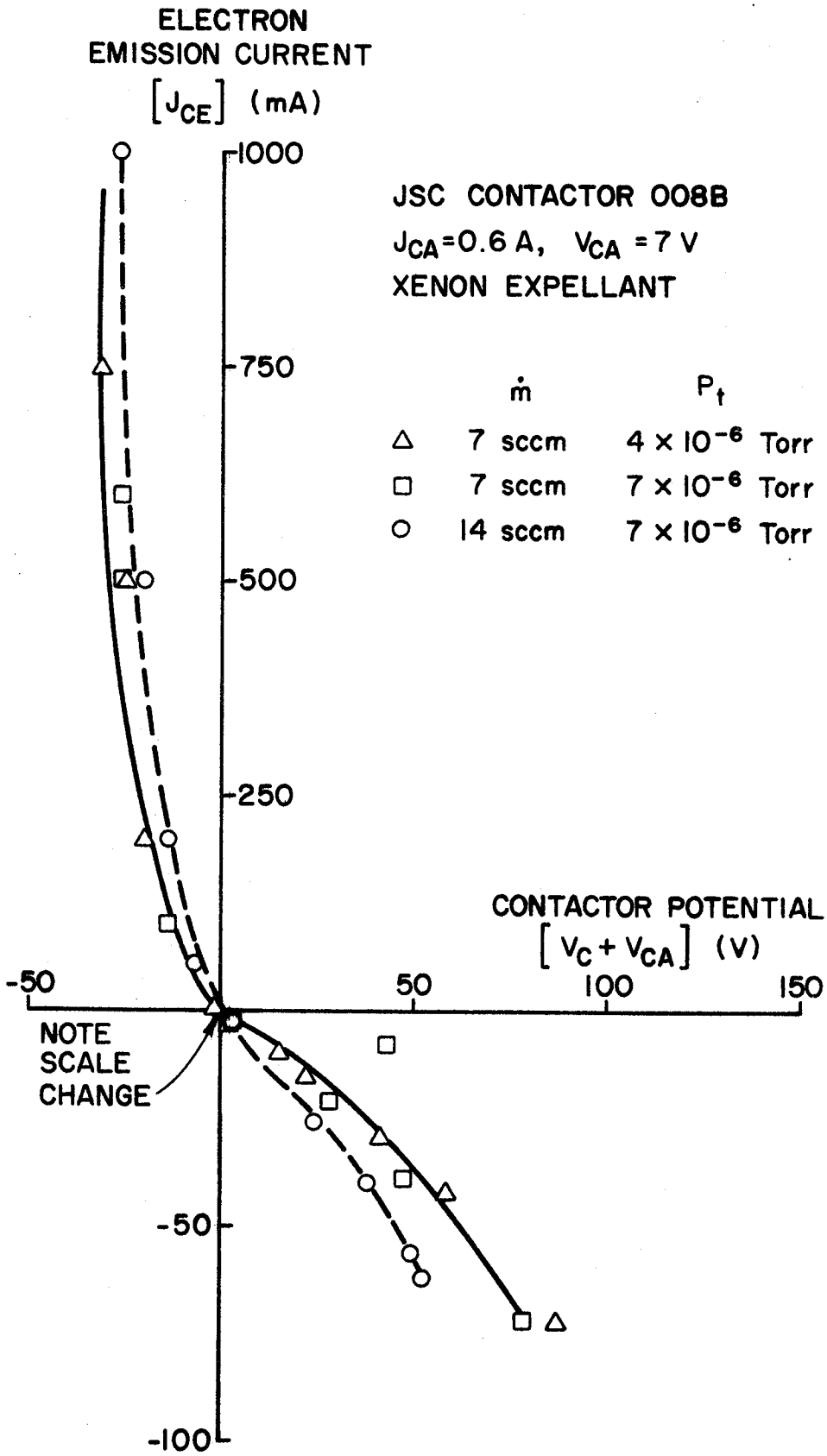

Fig. 21 Contactor 008B Performance Characteristics
Effect of Background Pressure and Flow - Xenon

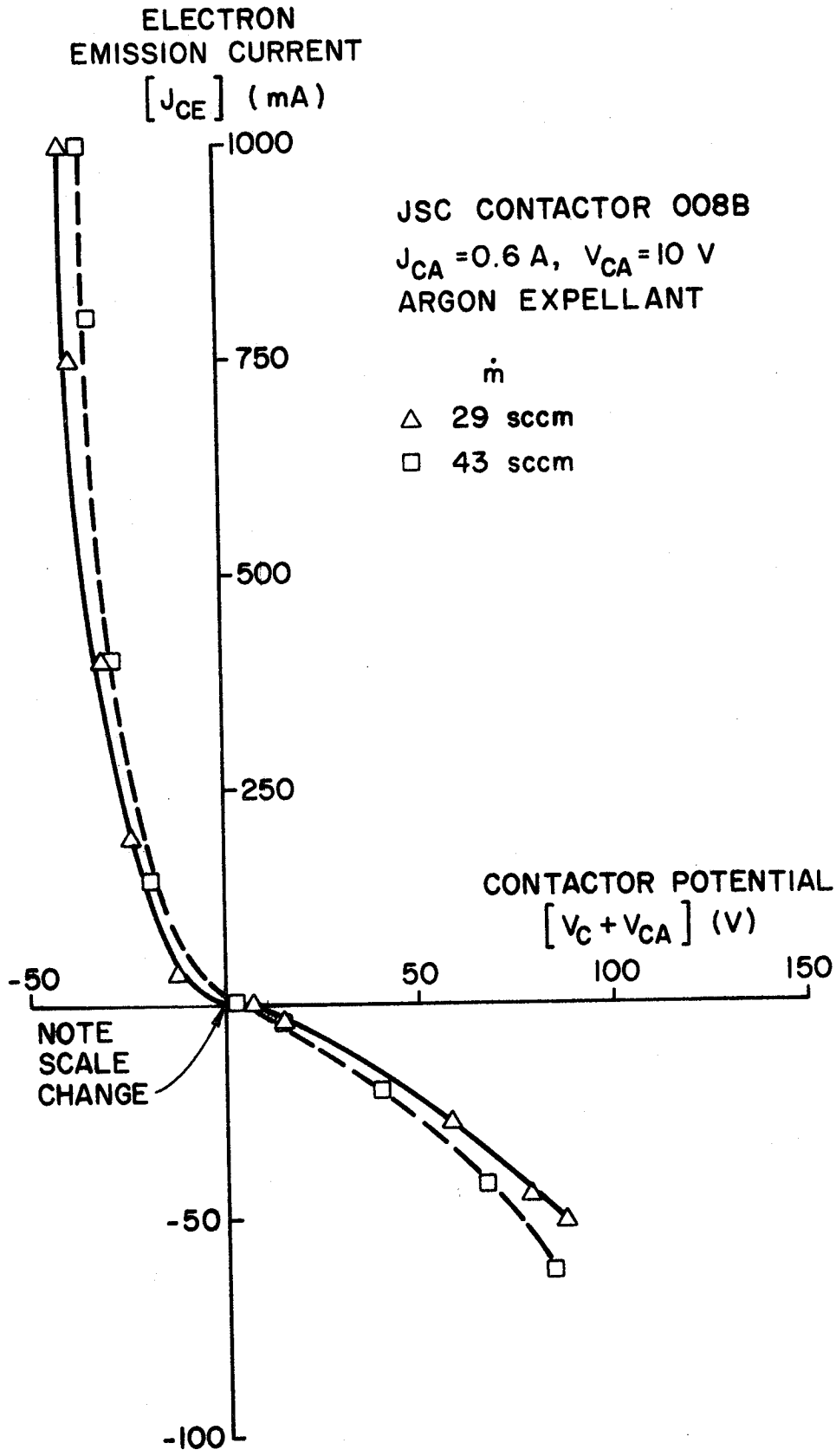

Fig. 22 Contactor 008B Performance Characteristics on Argon

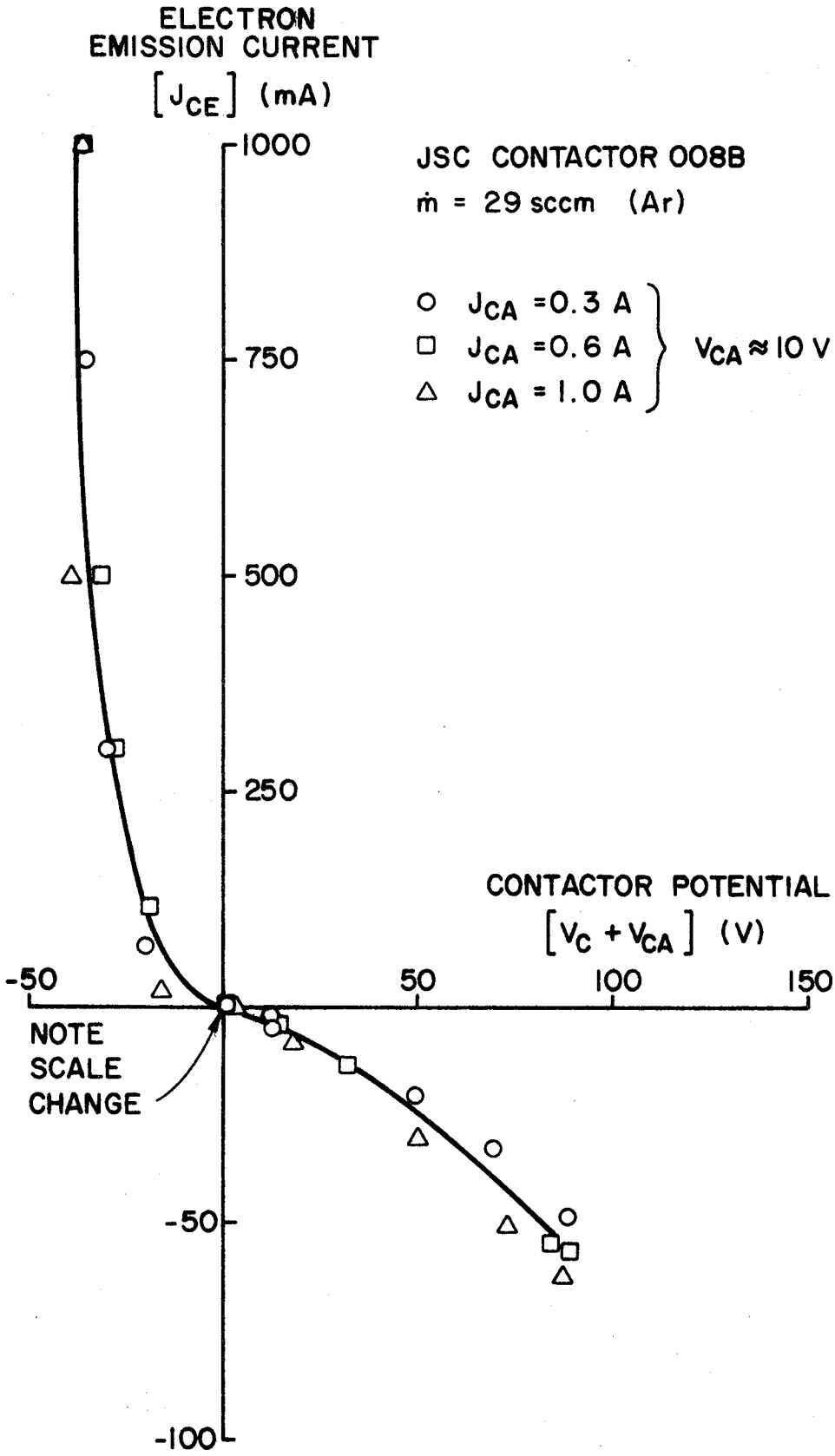

Fig. 23 Contactor 008B Performance Characteristics
Effect of Anode Current - Argon

contactor discharge (ion production rate) is examined as a function of discharge power and flowrate in Fig. 24. These data again show poorer performance with argon than xenon and the results are similar to those results presented in Fig. 16 for contactor 007B.

Ring Cusp Plasma Contactor Study

Experimental results obtained so far indicate that hollow cathode based contactors are very effective electron emitters but less effective electron collectors. The ring cusp ion source was built in an attempt to improve the electron collection capability of a contactor by improving its ion production ability. In order to understand the extent to which this had been accomplished, the performance of a conventional hollow cathode (Fig. 3a) was compared to the performance the ring cusp discharge chamber shown in Fig. 4 when it utilized this same hollow cathode as its electron source. Figure 25 shows a typical comparison between the performance curves for these contactors which were obtained with 1.4 sccm of xenon expellant flow through the hollow cathode at similar discharge powers. The simulator was turned off while collecting these data so the curves display only the electron emission and ion emission characteristics of the contactors. It is apparent from the curves, however, that substantial electron currents can be emitted to the tank at modest contactor potential differences so in the electron emission mode it is concluded that both contactors perform satisfactorily. The striking difference between the two curves in Fig. 25 is the greater ion current that can be drawn from the ring cusp contactor (approximately 10 mA) compared to the conventional hollow cathode (less than 1 mA) at about a 60v contactor potential. To compare these two contactors, curves similar to the ones shown in Fig. 25, were obtained for both argon and xenon expellants at various power levels and flowrates.

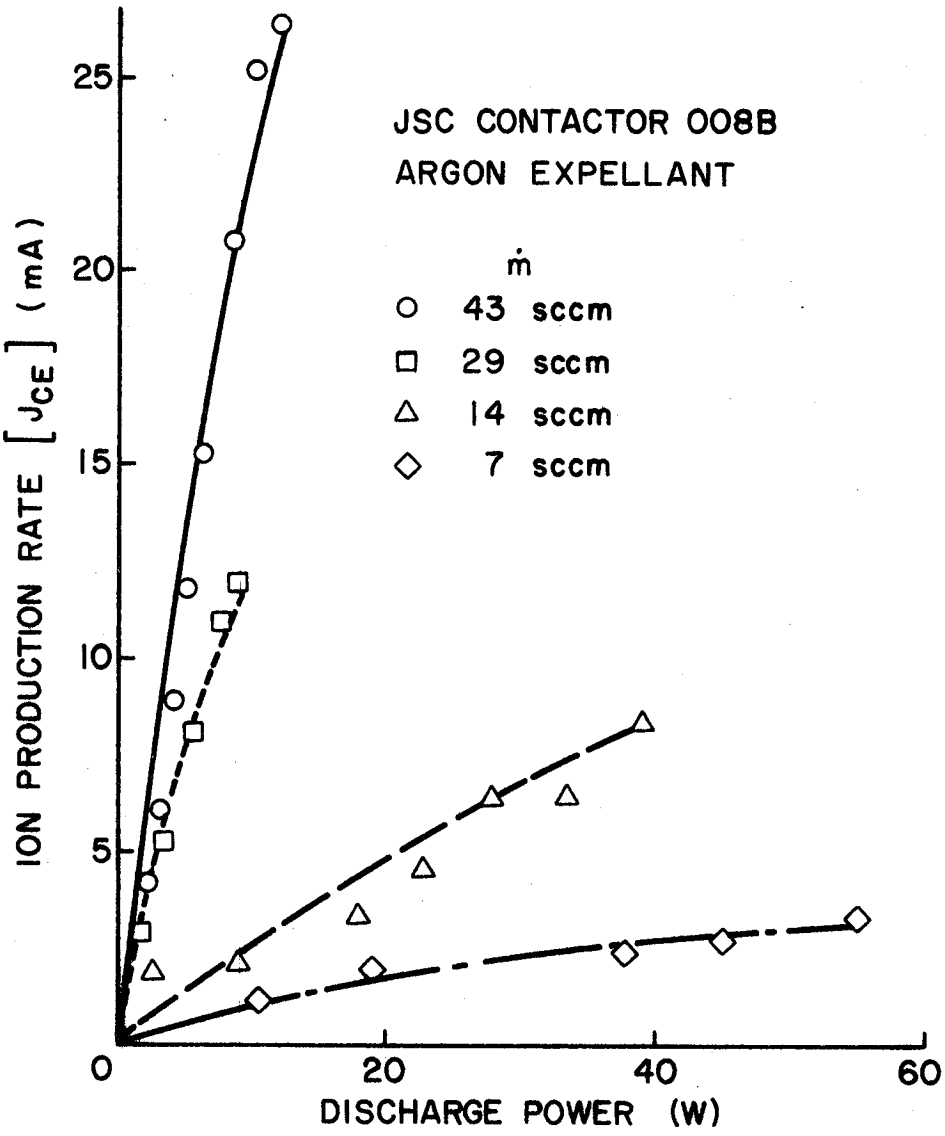

Fig. 24 Effect of Argon Flowrate on Ion Production

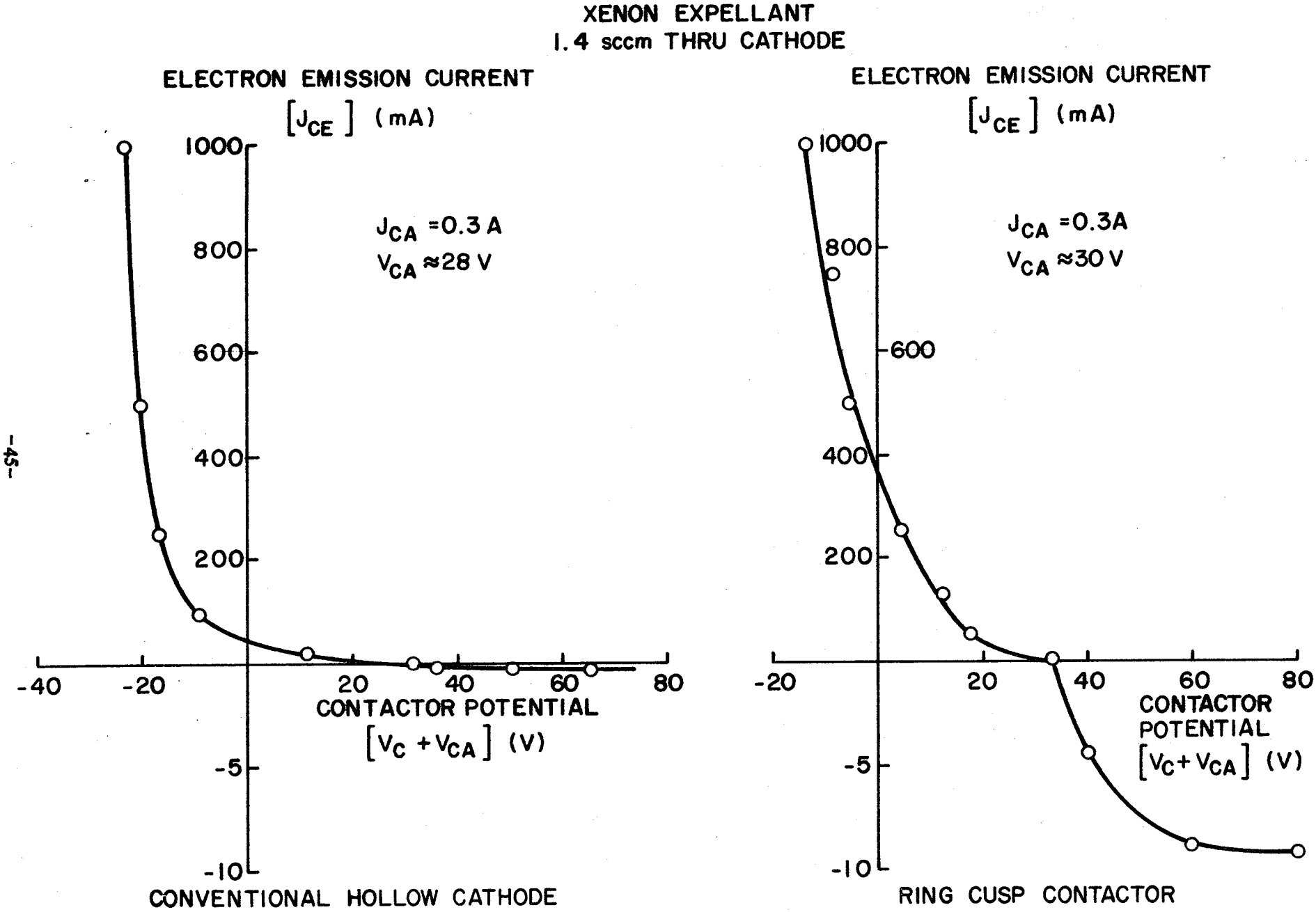

Fig. 25 Performance Curve Comparison

Because large electron emission currents could be effected at all operating conditions further comparison of the two sources will consist only of comparing their ion production capabilities (i.e. the ion current emitted from the source at a contactor potential greater than about 70v).

Figure 26 shows a comparison of the ion production capabilities of these two contactors operating on xenon expellant as a function of discharge power. The most important revelation of this figure is that the ring cusp contactor produces in excess of an order of magnitude more ion emission current than the conventional hollow cathode contactor when both are operating at identical power and flowrate levels. This figure also shows that the ring cusp contactor performs best when most of the flow is directed through the main flow plenum rather than through its hollow cathode. This was expected because atoms flowing through the hollow cathode tend to be directed toward the extraction aperture and, would therefore be expected to have a shorter residence time in the ionizing electron cloud of the discharge chamber than those entering through the reverse flow plenum. This figure also shows that the ion production capability saturates when the expellant flowrate through the hollow cathode becomes too large with either device.

Figure 27 shows a similar comparison to the one given in Fig. 26 but the data of Fig. 27 were obtained on argon expellant. Comparison of Figs. 26 and 27 shows degraded ion production capabilities for both the conventional hollow cathode contactor and the ring cusp contactor when they are switched from xenon to argon expellant. Further the trends just identified in Fig. 26 for xenon are also observed for argon. Using the data of Figs. 26 and 27 one can compute the energy cost of an ion produced in the plasma contactor and extracted from it as a function of the fraction of the

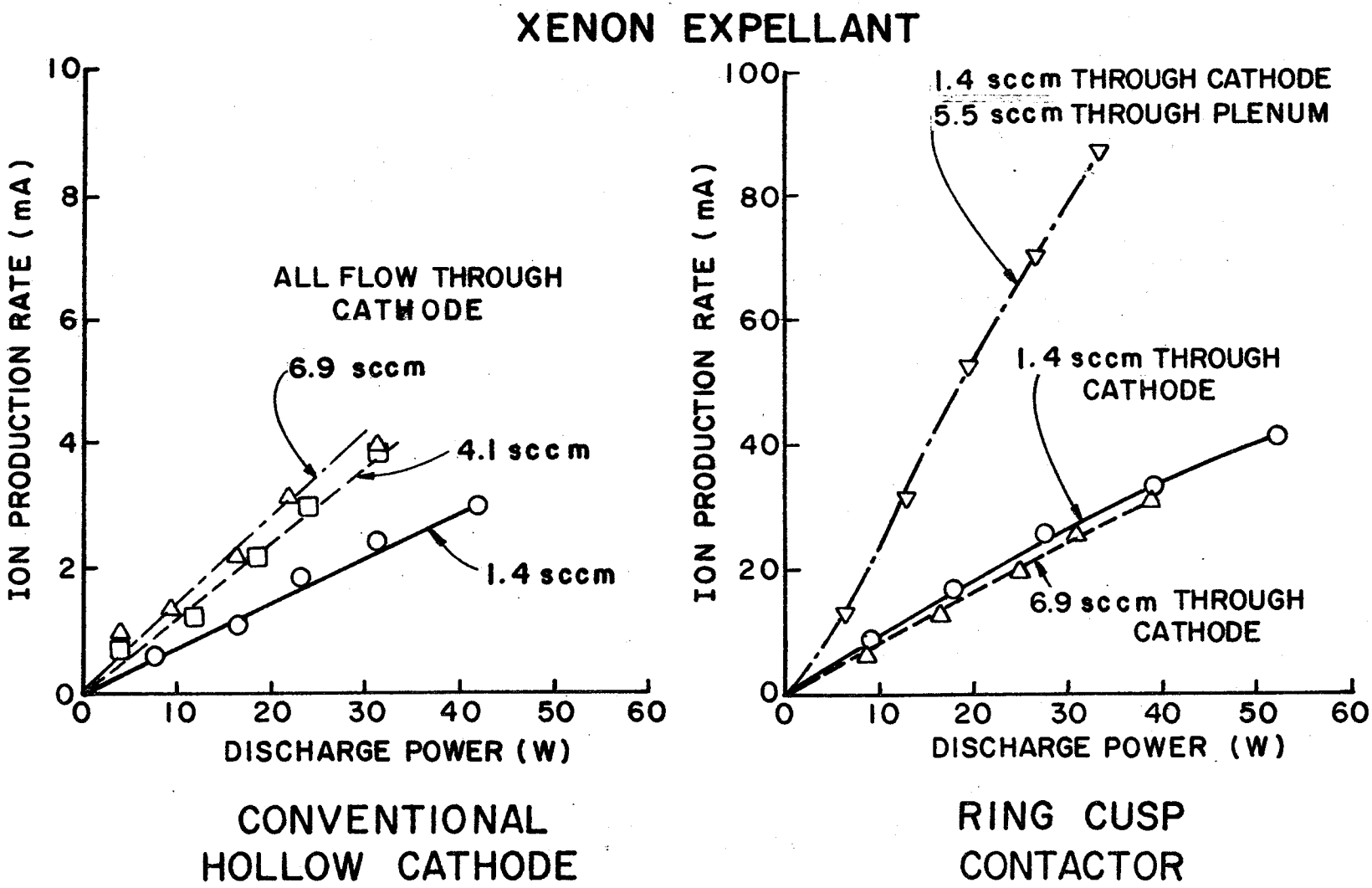

Fig. 26 Ion Production Rate Comparison - Xenon

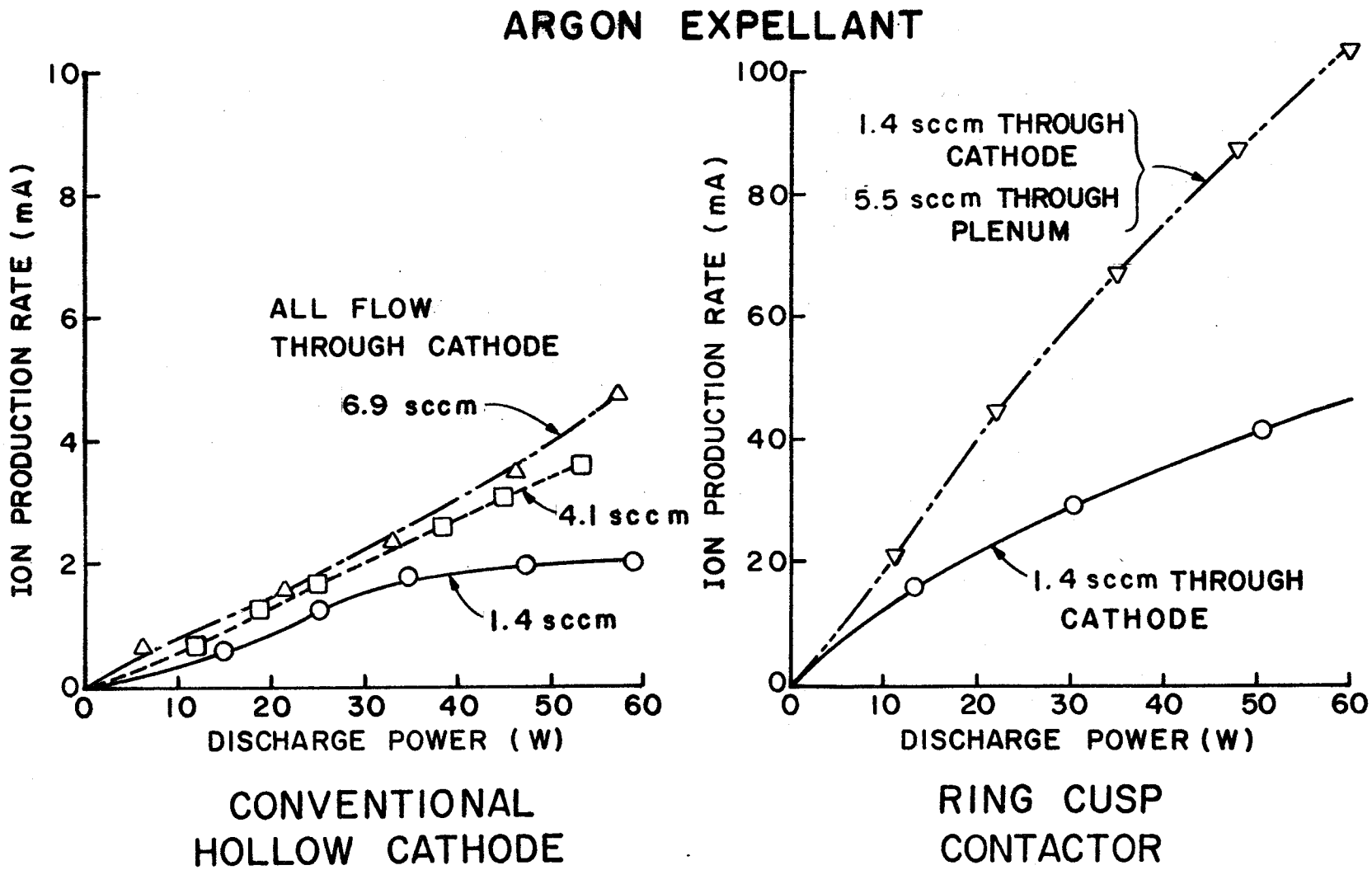

Fig. 27 Ion Production Rate Comparison - Argon

expellant fed into these contactors. These two performance parameters which are used to characterize ion thrusters[5] are plotted against each other in Figs. 28 and 29 for the two contactors operating on xenon and argon respectively. Comparison of these plots indicates the following:

- o The ring cusp contactor performs much better than the conventional hollow cathode in terms of both extracted ion energy cost and expellant utilization. In this regard note that the scale on the energy cost axes for the ring cusp contactor are an order of magnitude below those for the conventional hollow cathode.
- o Operation on xenon yields lower extracted ion energy costs and higher expellant utilizations than operation on argon does.
- o In order to realize the best performance of the ring cusp contactor it is preferable to inject most of the expellant through the main flow plenum rather than through the hollow cathode.

The curves in Figs. 28 and 29 have not reached the utilization level where they begin to show a rapid increase in energy cost per extracted ion. Consequently they suggest that the ring cusp contactor could be operated at considerably higher powers than it has been in obtaining these data. This in turn suggests that higher expellant utilizations could be achieved without introducing significant increases in extracted ion energy cost for this contactor.

A set of tests were performed to optimize ring cusp contactor performance by varying the open area of the extraction aperture shown in Fig. 4.[7] When this was done and the contactor was operated in conjunction with the simulator so electrons could be drawn from the simulated space plasma, curves of the type shown in Fig. 30 were obtained. The optimum extraction aperture diameter in this study was found to be 5.5 cm. Figure 30 shows

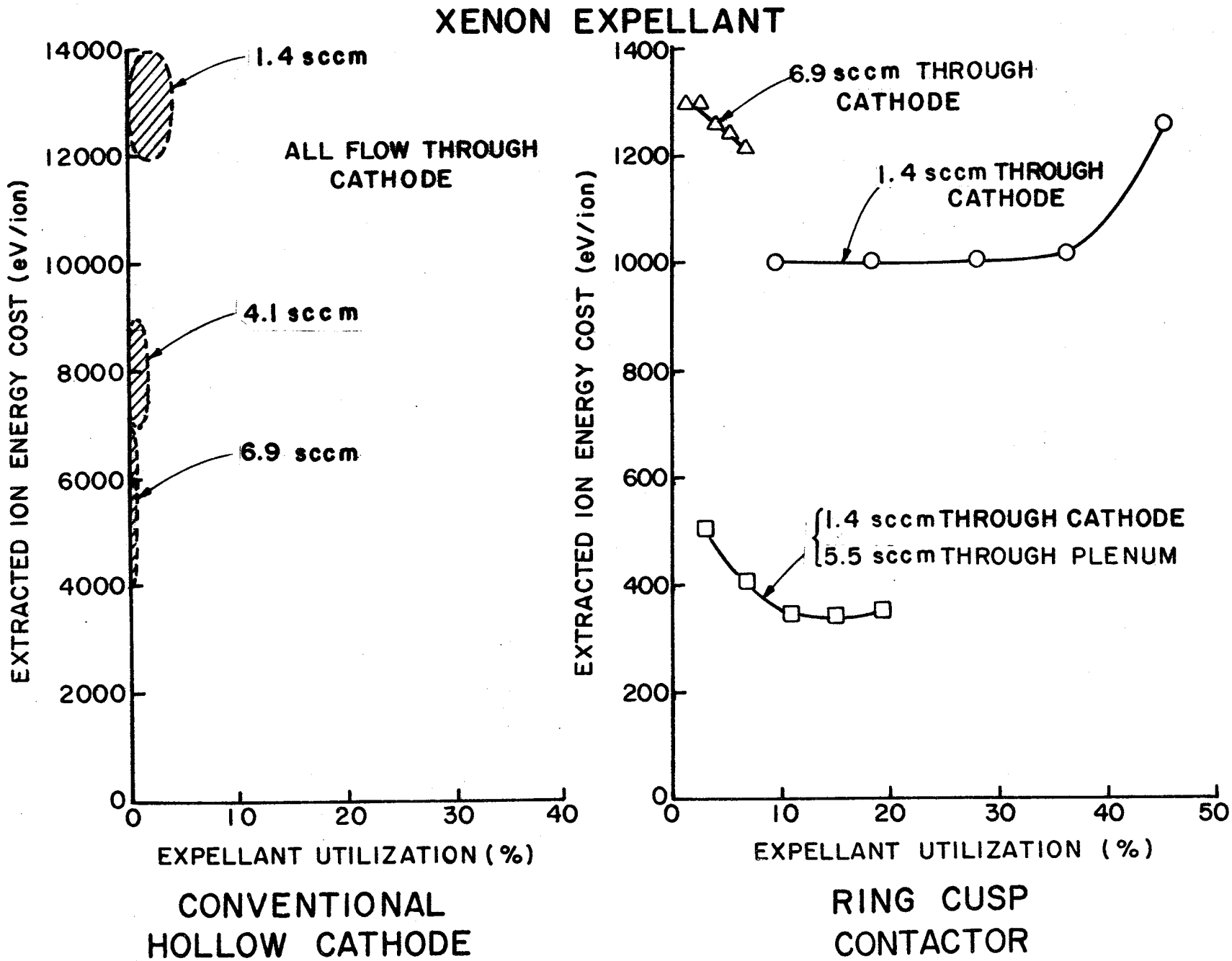

Fig. 28 Ion Production Performance Comparison - Xenon

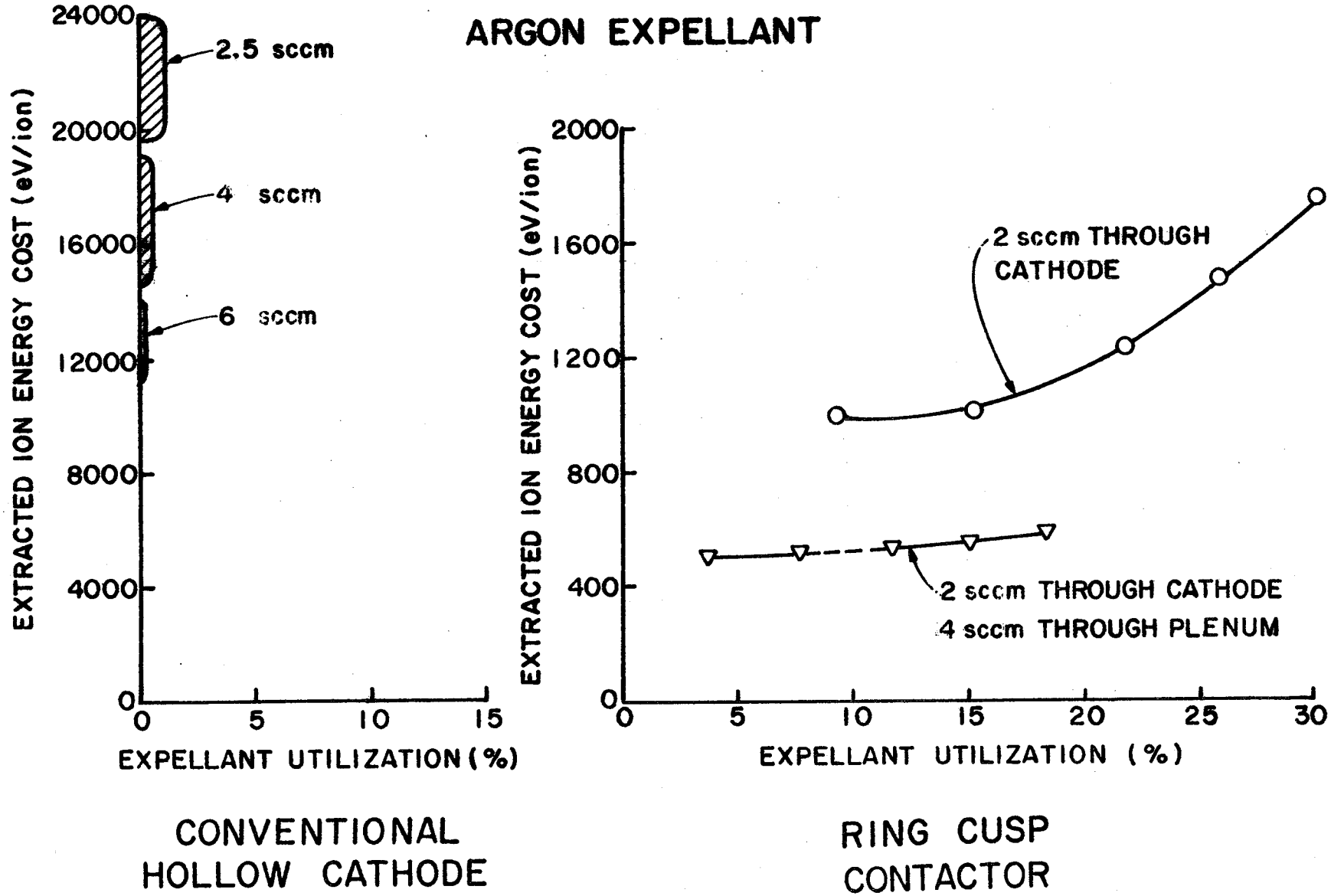

Fig. 29 Ion Production Performance Comparison - Argon

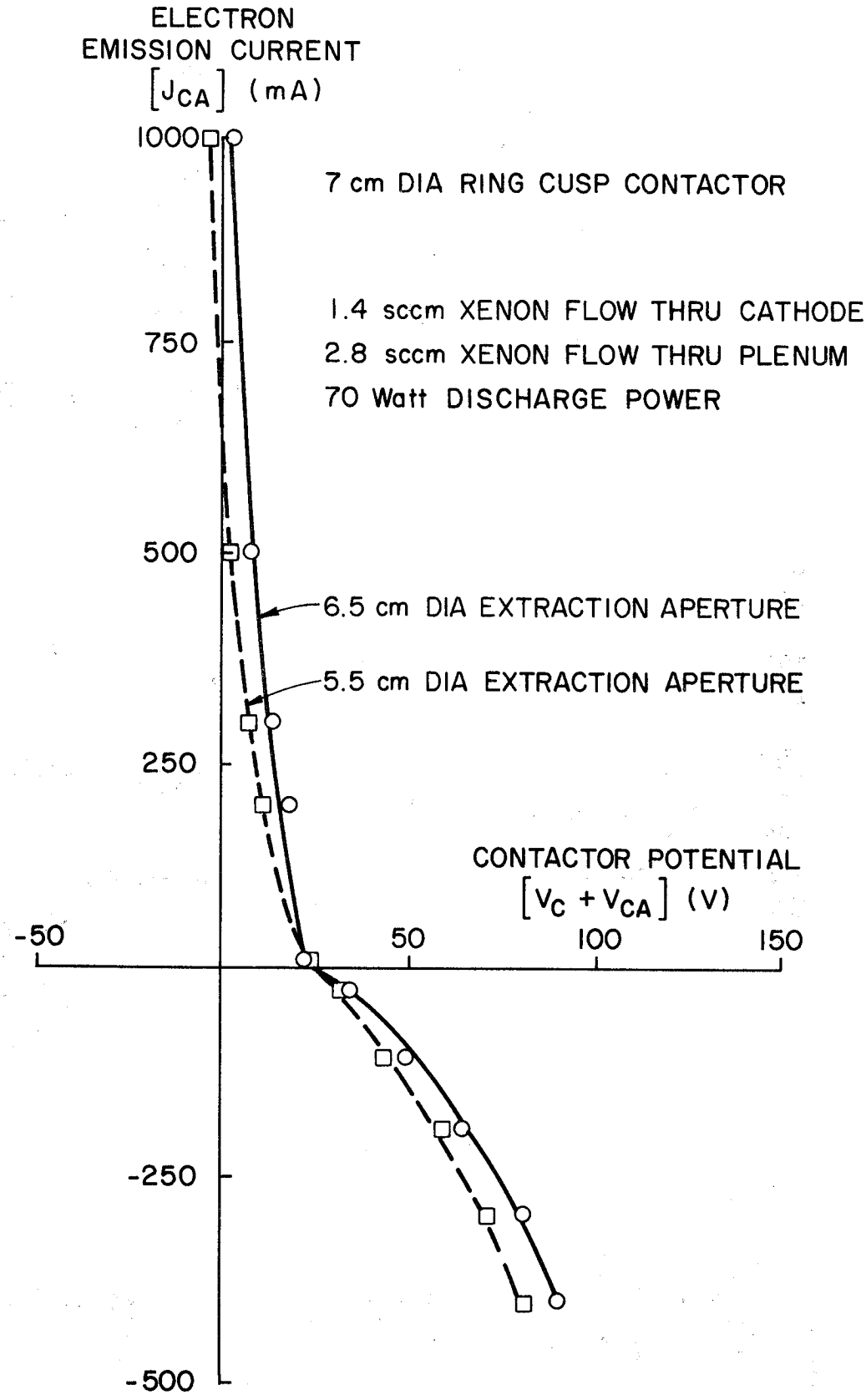

Fig. 30 Ring Cusp Contactor Performance

the comparison of the data for the 6.5 cm aperture used to obtain the data in Figs. 25 through 29 along with the optimum 5.5 cm diameter extraction aperture. This contactor operates from an electron emission current of 1000 mA to an electron collection current of about 500 mA as the contactor potential is changed by about 70v at a modest (4.2 sccm) xenon flowrate. The potential drop that would be expected in a space situation between the contactor anode and the space plasma would be expected to be about two-thirds of the range shown in Fig. 30 (~50 v).

Extended Anode Contactor Performance in the Ignited Mode

A set of tests performed during the grant period using the JSC high current contactor and another set of tests performed after this period using JSC contactor 017B yielded particularly good performance data. Contactor 017B has an extended anode design like the one shown in Fig. 3b for contactors 007B and 008B. The results associated with the first of these tests are shown in Fig. 31. At the time these results were obtained the simulator emission current was not monitored carefully to assure that it agreed closely with the contactor emission current. Further, the ignited mode of electron collection had not been identified and defined so it is not known for certain if the contactor was operating ignited. Based on more recent tests it is believed that it was operating in the ignited electron collection mode. Certainly in the ignited mode data similar to that shown in Fig. 31 has been observed.

The data shown in Fig. 32 were obtained at a high contactor flowrate and in the case of the circular symbols and the dotted line with a second JSC extended anode contactor (020B) operating at a high flowrate (7 sccm) as the simulator in place of the usual simulator. While the performance suggested by the curves of Figs. 31 and 32 is good it must be noted that

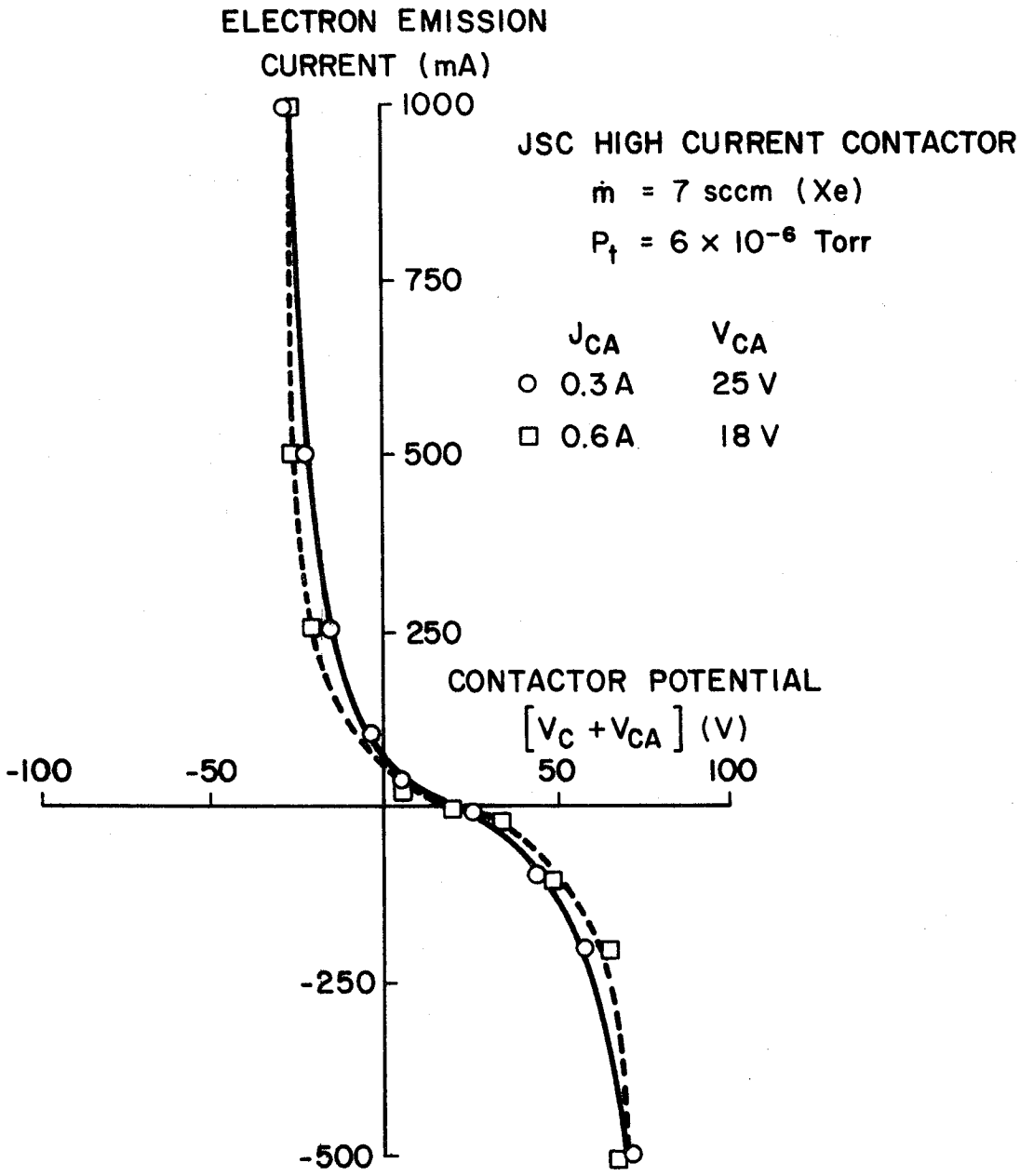

Fig. 31 Performance Characteristics -
Probable Ignited Mode Current Collection

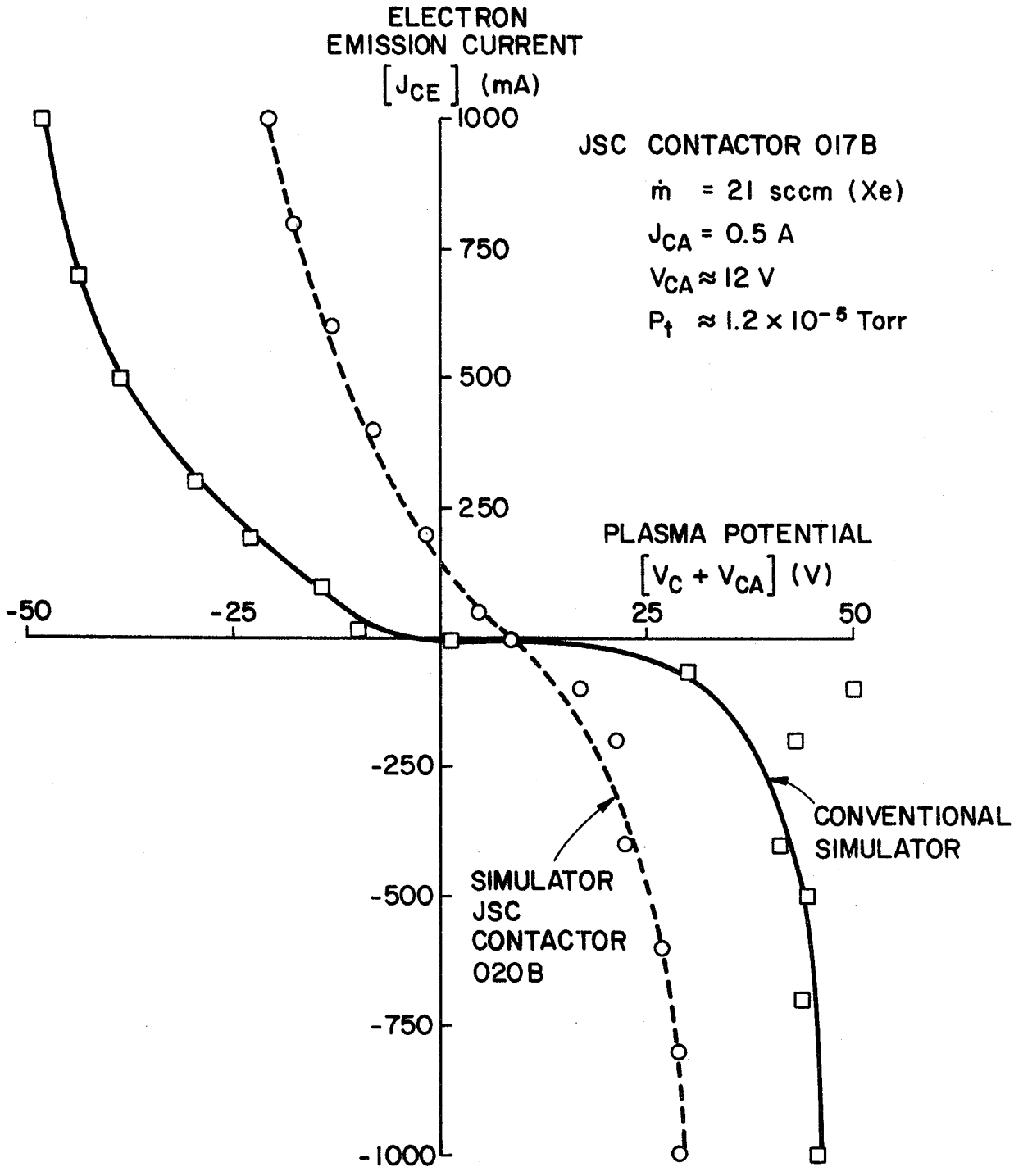

Fig. 32 High Flow, High Ambient Density Plasma Performance Characteristics

they were obtained at high flowrate, tank pressure and plasma density conditions that are probably not representative of the ambient conditions expected during most space tests.

More data collection, analysis and evaluation is considered necessary before any definitive statements can be made about the performance that contactors operating at conditions like those associated with Figs. 31 and 32 would exhibit in space. These curves do indicate that there is at least the potential for achieving high electron collection current, low voltage drop operation with hollow cathode contactors utilizing the extended anode design.

CONCLUDING REMARKS

Studies conducted to date have shown that the hollow cathode based contacting devices are well-suited to the plasma contacting process. They are particularly well-suited to electron emission. They exhibit good performance because they produce both electrons and low-energy ions which form a high density plasma plume around the contactor. Any of the contactors investigated in this study should be suitable to emit electron currents over 1 A and collect them in the 100 mA range at driving potential differences below about 100 v. The extended anode and ring cusp contactors perform better as electron collectors. Although more tests are considered to be necessary to demonstrate that they would collect electron currents from a dilute space plasma at levels as high as 1 A, data obtained at high tank pressure and electron density levels did yield collection currents in this range. All contactors were observed to perform better on xenon than on argon. The extended anode and ring cusp contactors operating on xenon appear to have adequate electron collection capabilities for the Hitchhiker-G and 2 kW PMG/POF experiments. One concern that was identified

with the extended anode contactor relating to the conduct of short duration space tests was a concern associated with its restart ability. Several tests suggested that its insert tended to become either contaminated or depleted of low work function material during operation. This may have been due to prolonged testing at JSC prior to their operation at Colorado State University. It did appear that they tended to be operated at high flowrates where cathode interior pressures and very small emission region spot sizes would be expected. Operation in this regime would be expected to overheat and deplete the insert of low work function material.

The model presented in Appendix B indicates that the maximum electron current that can be collected by a contactor at a given driving potential difference may be limited by the rate at which ions can be extracted from the high density plasma plume produced by the contactor. Thus, contactor ion production may become the performance limiting phenomenon at high electron collection current operating conditions. Because the extent to which operation at high electron collection currents in a ground-based facility is limited by tank perturbation and excessive simulated plasma density conditions it is difficult to design a straightforward experiment that is a valid simulation at the maximum electron collection current levels that could be achieved in space. Hence the ion production capability of a contactor has been used as an indicator of the relative performance that could be expected at high electron collection currents. In general the tests performed showed that increasing the ion production rate of a contactor by increasing contactor anode current or flowrate did not improve its electron collection performance substantially. This suggests that performance was not limited by the ion production rate over the range of experimental conditions investigated. However, ion production capability may still be the

limiting factor at higher electron collection current levels.

REFERENCES

1. Sisson, J. M. "Development Status of First Tethered Satellite System," AIAA Paper 86-0049, Jan. 6-9, 1986, Reno, Nevada.

2. Siegfried, D. E., and P. J. Wilbur, "A Model for Mercury Orificed Hollow Cathodes: Theory and Experiment," AIAA Journal, V. 22 Oct. 1984, pp. 1405-1412.

3. McCoy, J. E., "Electrodynamic Plasma Motor/Generator Experiment," Paper from NASA/AIAA/PSN Int'l. Conf. on Tethers in Space, Sept. 17-19, 1986, Arlington, Va.

4. McCoy, J. E., " Plasma Motor/Generator Reference System Designs for Power and Propulsion," Paper from NASA/AIAA/PSN Int'l. Conf. on Tethers in Space, Sept. 17-19, 1986, Arlington, Va.

5. Brophy J. R., and P. J. Wilbur, "Simple Performance Model for Ring and Line Cusp Ion Thrusters," AIAA Journal, v. 23, Nov. 1985, pp. 1731-1735.

6. Wilbur, P. J. and J. D. Williams, "An Experimental Investigation of the Plasma Contacting Process," AIAA Paper 87-0571, Jan. 12-15, 1987, Reno, Nevada.

7. Williams, J. D., "Electrodynamic Tether Plasma Contactor Research" appears in "Advanced Electric Propulsion and Space Plasma Contactor Research - 1986," P. J. Wilbur, ed., to be published.

8. Whipple, E. C., "Potentials on Surfaces in Space," Reports on Progress in Physics, v. 44, 1981 British Institute of Physics, p. 1237.

9. Parks, D. E., and I. Katz, "Theory of Plasma Contactors for Electrodynamic Tethered Satellite Systems," Applications of Tethers in Space Workshop, Venice, Italy, Oct. 15-17, 1985.

10. Wei, R., and P. J. Wilbur, "Space-charge-limited Current Flow in a Spherical Double Sheath," J. Appl. Phys., v. 60, 1 Oct. 1986 pp. 2280-2284.

11. McCoy, J. E., "200 kw Electrodynamic Power Plasma Motor/Generator (PMG) Systems Study," Proceedings: Tether Applications in Space Program Review, McLean, Virginia, July 17-18, 1985, pp. 141-181.

12. Kerslake, W. R., "SERT II Thrusters - Still Ticking after Eleven Years," AIAA PPaper 81-1539, Joint Propulsion Conference, July 27-29, 1981, Colorado Springs, Colorado

13. Siegfried, D. E. "Xenon and Argon Hollow Cathode Research" appears in "Advanced Ion Thruster Research" NASA CR-168340, P. J. Wilbur ed, Jan. 1984, pp. 76-121.

14. McCoy, J. E. private communication to P. J. Wilbur, Feb. 10, 1987.

APPENDIX A

PLASMA CONTACTOR SELECTION CONSIDERATIONS

In general ideal plasma contactors best suited to high current applications like those associated with electrodynamic tether missions would tend to have the following characteristics:

1. Compatibility with the host satellite and its associated mission.
2. High electron production capability.
3. High ion production capability.
4. High reliability (for starting and operation).
5. Passive ion and electron emission control.
6. Switchover capability (between electron emission and electron collection).
7. Low ion and electron energies.
8. Low system mass and size.
9. Low expellant consumption rate.
10. Low operating power consumption rate.
11. Rapid startup capability.
12. Simplicity.
13. Low system cost.
14. Performance capability independent of host satellite orientation relative to magnetic field and vehicle velocity vectors.

Some interpretation and discussion of the meaning of some of these items is necessary. The compatibility requirement (1) suggests, for example, that any expellant required by the contactor would not result in damage or loss

in sensitivity of instruments being used on the host satellites. High ion and electron production capabilities relate to the contactor's ability to establish the desired low impedance connection; the capabilities are the major focus of the research discussed in the body of this report. Passive emission control (5) suggests the need for a device which will automatically accommodate changes in tether output current and voltage without requiring adjustments to such contactor operating parameters as contactor power or expellant flowrate. Switchover capability (6) is the term used to describe the process of changing the tether operating mode between power generation and thrust production. When this occurs the direction of current flow in the tether will be reversed and thus a plasma contactor, which could have been operating in the electron collection mode, would have to switch to the electron emission mode. It is desirable that this switchover be automatic and require no operator attention to the contactors. The requirement for low ion and electron energy (7) relates to the need for efficient system operation. The low system mass and size and expellant consumption rate characteristics (8 and 9) must be viewed in comparison to the mass and size of other system components and they should be small in this sense. Characteristic (10) relates to any auxiliary power required to operate the contactor as well as tether generated power dissipated as a result of voltage drops produced in the space plasma/contactor plasma interface region. All the other items in the list of contactor characteristics are considered self-explanatory.

Plasma contactor performance can be characterized by a plot of contactor electron emission current vs. contactor potential measured relative to space plasma potential. The ideal plasma contactor would exhibit a characteristic curve appearing as a vertical line on such a plot. This ideal

contactor (which has zero impedance and behaves like a copper grounding wire) supplies sufficient ions and/or electrons to conduct any current demanded while holding the contactor at space plasma potential as Fig. A1 suggests. Such performance might be approached by having an ion/electron production rate that would cause the plasma plumes identified in Fig. 1 in the body of this report to have a high density (high conductivity) and a surface area equal to or greater than the tether current divided by the ambient space plasma current density.

Ion and electron guns are suggested occasionally as plasma contactors but their characteristics (shown dashed on Fig. A1) are not indicative of low impedance devices and they are therefore not well suited to this application. Their emission capabilities are limited to their maximum design beam currents (J_{eg} and J_{ig}), they are not switchable (both an ion and an electron gun would be required at each end of the tether) and they would require active control to prevent inadvertent charging to high positive or negative potentials. Such potentials would be limited only by electron or ion accelerating potentials associated with the guns (V_{es} or V_{is}) or electron/ion currents that could be drawn from the space plasma to conducting surfaces on the spacecraft. These spacecraft charging potentials can be sufficient to cause damage to spacecraft instruments as Whipple[8] has pointed out. Finally the guns are not efficient plasma contactors because they consume power unnecessarily in the process of accelerating their ion/electron beams.

While approaching the vertical characteristic curve shown in Fig. A1 is desirable, achieving this could require such a large contactor operating power (to get the required ion and electron current densities) that operation at a condition departing somewhat from this ideal characteristic might

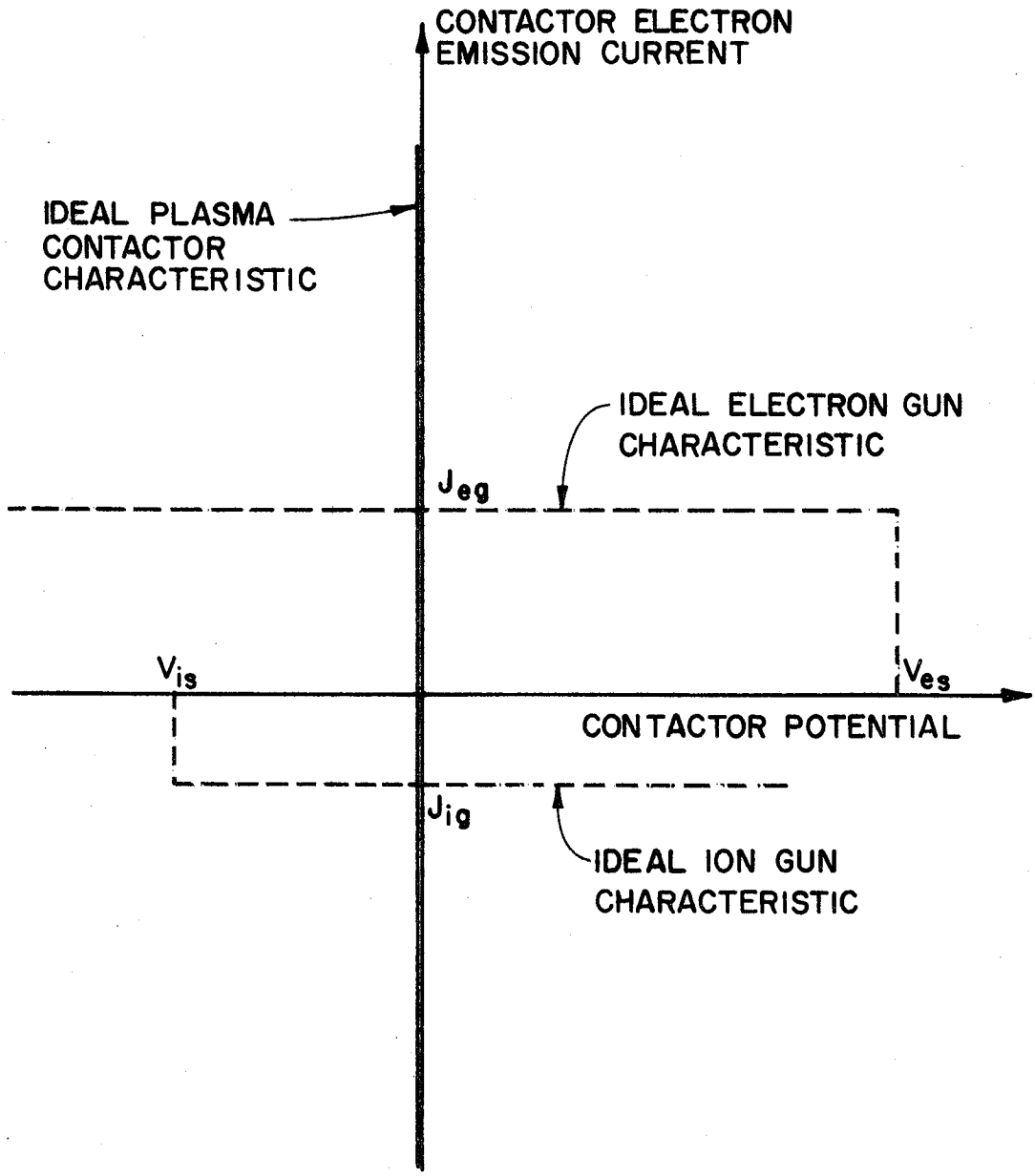

Fig. A1 Ideal Plasma Contactor Characteristics

be preferred. As Park, et al.,[9] have pointed out, reduction of the high density plume size below that sufficient to yield a negligibly small contactor voltage drop results in the development of a sheath between the high density plume region and the relatively unperturbed space plasma. This suggests the plasma contacting configuration shown in the conceptual sketch of Fig. A2. Here the high plasma density plume region is assumed to be such a good conductor that no potential difference develops between its outer surface and the plasma contactor anode located within the plasma source. A voltage drop does develop through the double sheath region, however, as electrons flow between the plasma source and unperturbed space plasma and ions flow in the opposite direction. Space charge effects limit the currents that flow in this situation under the influence of a prescribed voltage difference between the high density and space plasmas provided there are infinite sources of electrons and ions at the boundaries of the high density plasma source and unperturbed space plasma respectively. It should be noted that the configuration of Fig. A2 is reversible. Electrons produced in the plasma source can either flow radially outward while ions from the space plasma flow inward or electrons can be drawn from the space plasma while ions produced in the plasma source counterflow outward. These two modes of operation are designated the electron emission mode and the electron collection mode respectively.

A Theory of the Plasma Contacting Process

During the reporting period under partial support from the JSC grant, a simple theoretical model describing the basic elements of the plasma contacting process at the space-charge-limited operating condition was developed.[10] In this model it was assumed that spherical symmetry existed in the manner suggested by Fig. A3 and that a current (J_i), due to either

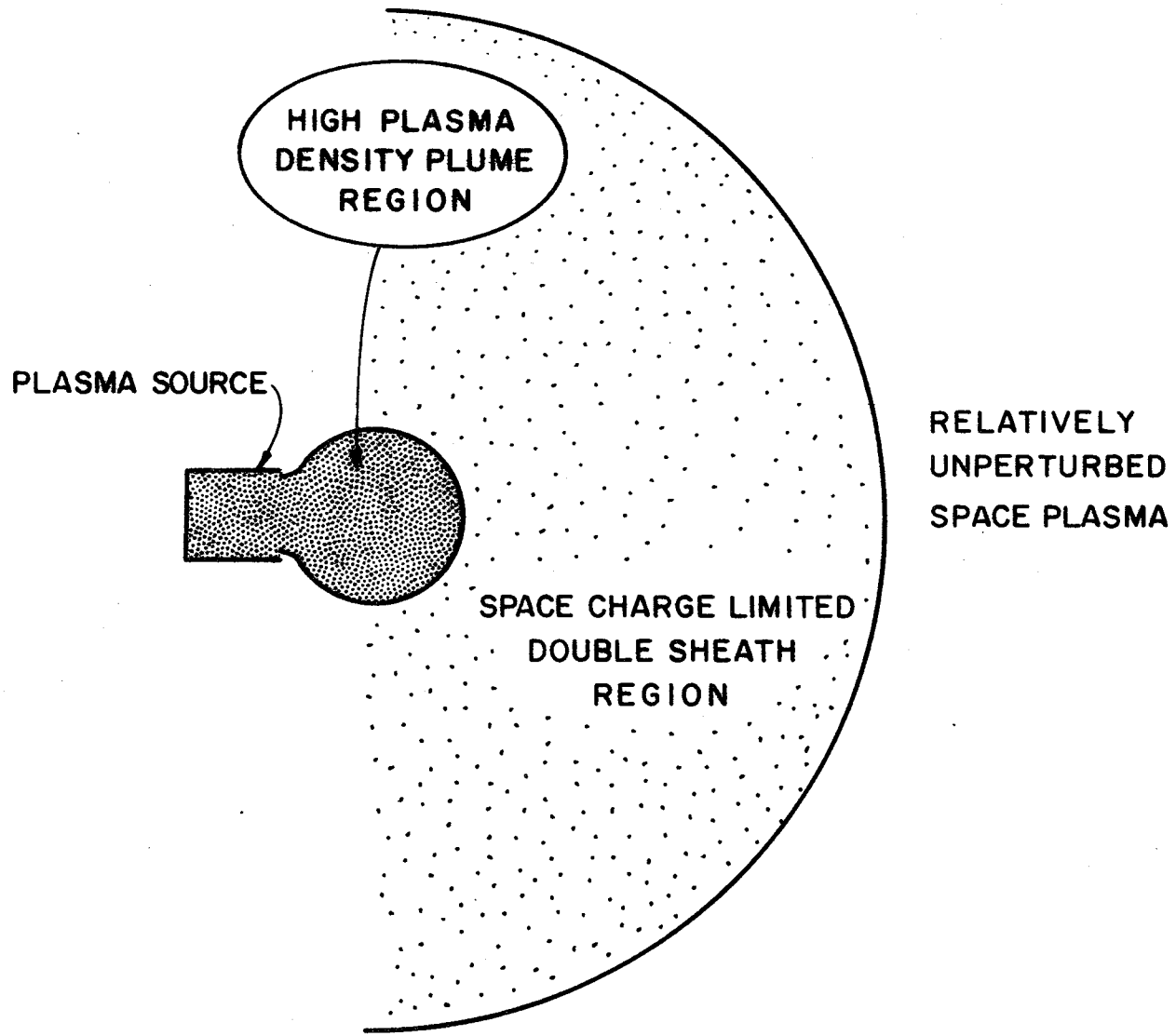

Fig. A2 Physical Picture of Contacting Process

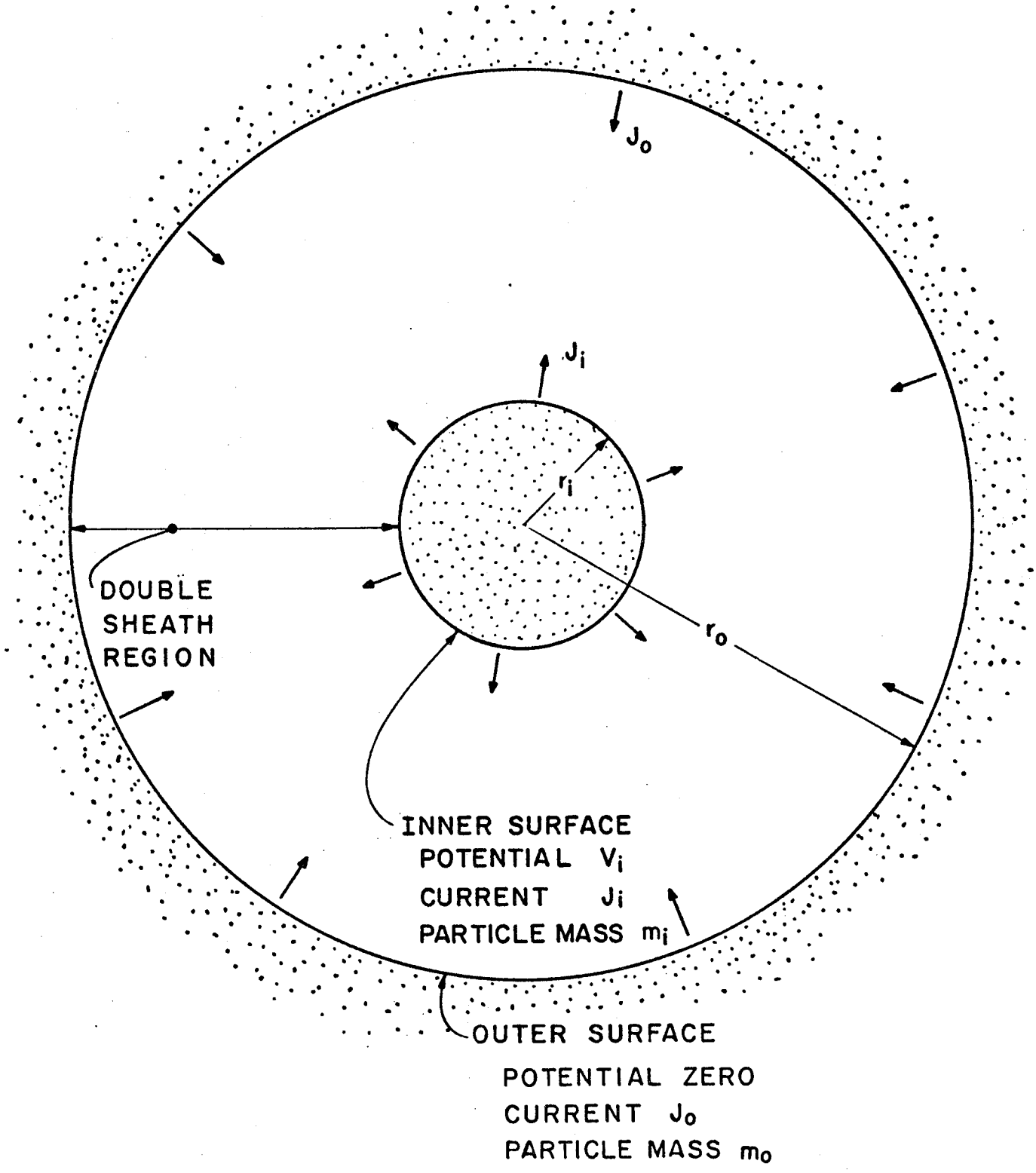

Fig. A3 Theoretical Model Concept

ions or electrons, was drawn from the inner surface at potential V_i. At the same time a counterflowing current of oppositely charged particles (J_o) was assumed drawn from an outer boundary at zero potential. The region between the equipotential surfaces where the voltage drop develops and the oppositely charged particles counterflow is referred to as the double-sheath region. While this simple model neglects the effects of electron and ion collisions both in terms of the impedance they induce and the production of additional ion-electron pairs, hopefully it will describe key features of the contacting process and be useful in computing the current conducted at a prescribed potential difference in the limiting case of a low electron collision frequency. The details of this development are included in the paper which is reproduced in Appendix B. The paper's key results, however, are equations describing the currents J_o and J_i which are reproduced here as Eqs. A1 and A2.

$$J_o = 4\pi\varepsilon_o V_i^{3/2}(2e/m_o)^{1/2} j_o \tag{A1}$$

$$J_i = \frac{J_o}{\alpha}\left(\frac{m_o}{m_i}\right)^{1/2} \tag{A2}$$

These equations are useful because they describe the currents that flow as a function of the masses of the charged particles flowing from the inner surface (m_i) and the outer surface (m_o), the voltage difference developed between the two surfaces (V_i), the constants e and ε_o and the parameters j_o and α. Values of these parameters are given as a function of the radius ratio r_i/r_o in Appendix B. If one assumes the system is operating in the electron collection mode, J_o would represent an electron current and J_i an ion current and these two currents would add together to give the total current flowing between the two surfaces. It is noteworthy that J_i is considerably less than J_o in the electron collection case because the ion mass

m_i is considerably greater than the electron mass m_o. The analysis of Appendix B shows that the importance of the ions to the conduction process is much greater than their direct contribution to the current. Their importance is reflected as an increase in the electron current over what would flow if the ions were not present to neutralize the electron space charge. In this regard, however, it should be noted that the model assumes infinite supplies of zero velocity electrons and ions at their source boundaries. It is noted that in the electron collection mode it is preferable to supply zero velocity ions to minimize the ion loss rate and therefore the required ion production rate of the plasma contactor.

It is suggested that a plasma contactor may always operate at the space-charge limited current flow condition defined by Eqs. A1 and A2 and that the radii r_i and r_o adjust themselves to assure that this occurs under the prevailing voltage difference, ambient space plasma and tether current conditions. It should be noted that the effects of the two phenomena neglected in the analysis, namely ionization and impedance inducing collisions, have contradictory effects. Enhanced ionization in the double-sheath region should enhance current flow at a given voltage difference while elastic collisions should reduce it.

Theory of Hollow Cathode Operation

A hollow cathode generating a neutral plasma discharge has been proposed as a simple plasma contacting device[11] that appears to have the characteristics identified previously as desirable. A schematic diagram showing the essential elements of a hollow cathode device and illustrating its key physical features is shown in Fig. A4. It consists of a small diameter (of order 1 cm) tantalum tube electron beam welded to a thoriated tungsten orifice plate. Located within and electrically connected to the

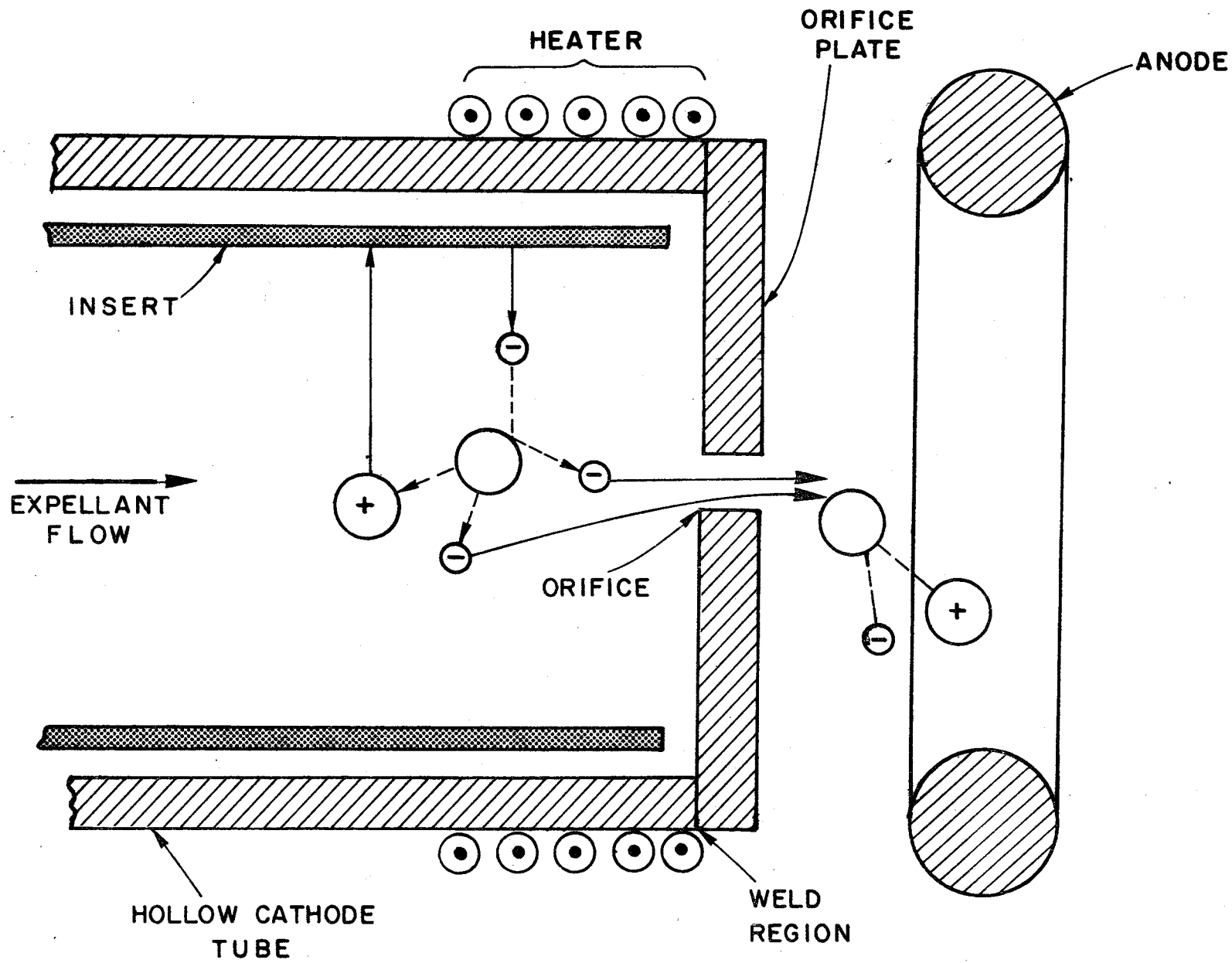

Fig. A4 Physical Features of a Hollow Cathode

cathode tube is a low work function surface (insert). An anode, located downstream of the hollow cathode and biased positive of the tube and insert, collects some of the electrons coming from the hollow cathode orifice thereby sustaining an electrical discharge and producing the desired plasma plume.

In order to initiate a hollow cathode discharge, expellant is fed through the hollow cathode tube and out of the orifice and the heater shown is energized to bring the insert to thermionic emission temperature levels. With the anode biased a few hundred volts positive of the insert electrons emitted from the insert surface are drawn toward the anode. Siegfried[2] has shown these electrons acquire sufficient energy as they pass through the plasma sheath adjacent to the insert surface to facilitate inelastic collisions with neutral atoms within the cathode tube. As a result of multistep processes these collisions result eventually in the production of ion-electron pairs. Both the primary electrons, from the insert surface and the secondary electrons derived from ionization find themselves unable to return to the insert, orifice plate or cathode tube surfaces because of the adverse potential gradients in the sheaths at these surfaces. Hence electrons remain in the cathode interior only until the anode or some other positively biased downstream surface or plasma draws them through the orifice. Positively charged ions on the other hand face an adverse potential gradient at the orifice and would not be expected to be drawn through it unless they could be carried along by the neutral expellant as a result of collisions. It is believed, however, that most ions are drawn to the insert surface, which they bombard with substantial kinetic energy. Because this bombardment heats the insert surface it is possible to turn the heater down or off once the discharge has started and the power associ-

ated with ion bombardment is available to sustain the insert temperature. The combination of the insert temperature and the potential gradient in the sheath at the insert surface sustains continued electron production through the field-enhanced thermionic emission mechanism. It is noteworthy that the cathode heater can be turned down or off after the cathode has started because this implies a substantial power reduction for a cathode that has been designed to sustain a low thermal power loss from its insert.

The potential difference across the orifice accelerates electrons passing through it giving them addition kinetic energy. They are therefore able to produce ion-electron pairs downstream of the orifice when they collide with atoms. The likelihood of this occurring is greatest near the orifice where neutral gas pressure associated with expellant flow through the orifice is highest. Neutral atom density drops off rapidly as the expellant gas expands in the region downstream of the orifice causing the electron mean free path for ionization to increase rapidly with distance from the orifice. Electrons coming from the orifice that don't have an ionizing collision in the orifice generally either escape or strike the anode and as a result the ionization efficiency for these electrons is low. Ions are produced downstream of the orifice at a sufficiently high rate, however, so the device may be classified as a plasma source rather than a simple electron source. It is believed that these ions play a critical role in the efficient operation of the hollow cathode as a plasma contactor in both the electron collection and electron emission modes of operation.

The orifice in the hollow cathode shown in Fig. A4 serves two main functions. First, it provides a current path allowing electrons to reach the downstream anode and contribute to the downstream plasma. Second, it restricts the expellant flowrate so the interior cathode pressure can be

sustained in the proper range without excessively high expellant consumption. A proper interior cathode pressure is important because it determines the length of the region on the insert from which electrons will be drawn.[2] If it is too low the electrons emitted from the insert will be unable to produce substantial numbers of electron-ion pairs through the multi-step collision process. The plasma sheath at the insert surface then becomes so thick that the field enhancement of the emission process is reduced. If the pressure is too high the length of the emission region on the insert is small, the insert overheats, loses its low work function coating and as a result degrades during operation. When the interior pressure is maintained in the proper range, however, the hollow cathode can serve as a very long lifetime,[12] efficient, high current electron source which also produces some ions and should serve as the basic element for a wide range of plasma contactors. The proper range for the cathode interior pressure is considered uncertain at this time. Siegfried[13] in his research on argon and xenon hollow cathodes using rolled foil inserts found that a pressure less than about 20 Torr was required to prevent the emission region from becoming so small that localized overheating of the insert resulted. McCoy[14] has stated, however, that cathodes with sintered tungsten inserts operate best at cathode internal pressures of about 100 Torr. The reason for this difference may be due to the fact that the sintered tungsten inserts conduct heat away from an emitting spot more readily thereby preventing the localized overheating observed by Siegfried.

Space-charge-limited current flow in a spherical double sheath

Ronghua Wei and Paul J. Wilbur
Department of Mechanical Engineering, Colorado State University, Fort Collins, Colorado 80523

(Received 31 March 1986; accepted for publication 16 June 1986)

Solutions to the problem of counterflowing, space-charge-limited, negatively and positively charged particle currents between two spherical surfaces are presented. They show that the current magnitudes exhibit the usual 3/2 power dependence on driving potential difference and square root dependence on particle charge-to-mass ratio. The magnitude of either current is strongly dependent on the radius ratio of the two spherical surfaces. The relative magnitudes of the two counterflowing currents are related by the square root of the mass ratio of the two charged particle species and a radius ratio factor that lies in the range ~0.1–1.0.

I. INTRODUCTION

When two concentrically located, spherical surfaces—each of which is a uniform source of low velocity, charged particles (one emitting positively charged particles and the other negatively charged ones)—are biased so the particles will counterflow through a vacuous region between the surfaces, a spherical double sheath will form. As the strengths of the two sources are increased, a condition will be achieved where further increases in the strength of either charged particle source will result in no further increases in the current passing between the surfaces. At this condition the sheath is said to be space-charge limited.

The solution to the space-charge-limited, spherical double-sheath problem is of interest because it describes the current flow between two cold plasmas which are biased relative to each other in spherical or spherical sector geometries. This situation may be observed, for example, in some cases where an electrodynamic tether contactor plasma is coupling to a space plasma[1] and in the case of a hollow cathode plasma coupling to the discharge chamber of an ion thruster.[2]

The space-charge-limiting effect has been studied extensively through the years. The early theoretical work was done primarily by Child and by Langmuir and co-workers who investigated the planar single sheath,[3] the planar double sheath,[4] and the spherical single sheath.[5] As far as the authors have been able to determine, however, neither Langmuir nor any subsequent researcher has published a solution to the spherical double-sheath problem which is addressed here.

II. PROBLEM FORMULATION AND SOLUTION

The basic elements of the spherical double-sheath problem are illustrated in Fig. 1. This figure shows an inner spherical surface (radius r_i) that is biased at a potential V_i and is a uniform source of charged particles. The outer spherical surface (radius r_0) shown is at zero potential and is a uniform source of oppositely charged particles. For this analysis all particles are assumed to be singly charged. Under the influence of the potential difference between the surfaces, particles of mass m_i from the inner surface are accelerated from a zero initial velocity toward the outer surface, and as a result a current J_i flows. Similarly, particles from the outer surface (mass m_0) start at zero velocity and are accelerated inward to produce the current J_0.

In order to facilitate the formulation of the problem, it will be assumed that the inner surface is a positively biased source of positive ions and the outer surface is a souce of negative particles (e.g., electrons). It is noted, however, that the final solution to the problem is general and valid both for the case of inward electron flow and outward ion flow under the influence of a positively biased inner surface, and for the case of outward electron flow and inward ion flow associated with a negative bias on this surface.

Poisson's equation, which describes the potential variation between the spherical surfaces, can be written

$$\nabla^2 V = -(e/\epsilon_0)(n_i - n_0). \tag{1}$$

For the spherically symmetric case under consideration here, Eq. (1) simplifies to

$$\frac{1}{r^2}\frac{d}{dr}\left(r^2\frac{dV}{dr}\right) = -\frac{e}{\epsilon_0}(n_i - n_0). \tag{2}$$

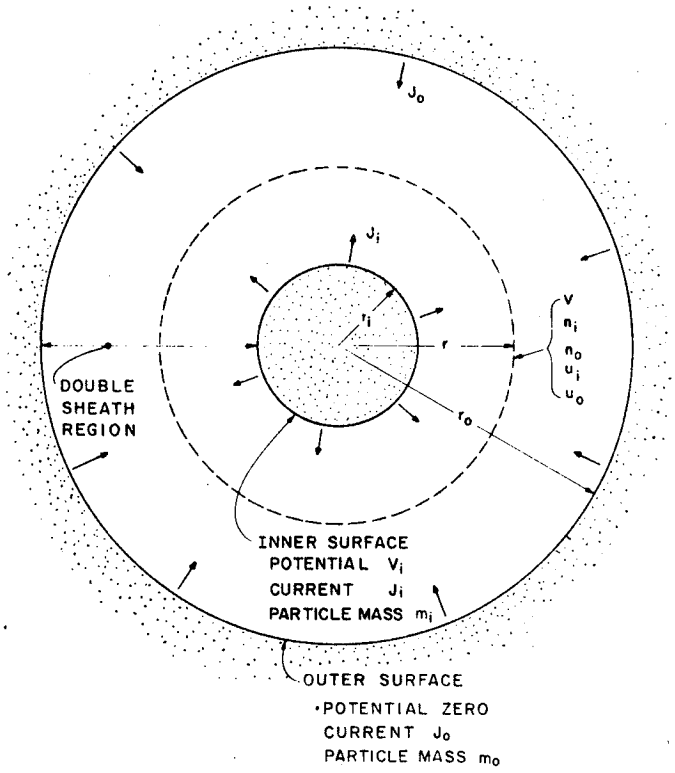

FIG. 1. Physical configuration.

 0021-8979/86/192280-05$02.40

In Eqs. (1) and (2) V is the potential at a spherical surface of radius r, where the particles from the inner surface have a density n_i and velocity u_i, and those from the outer surface have a density n_0 and velocity u_0 as suggested at the dotted line in Fig. 1. The symbols e and ϵ_0 represent the electron charge and the permittivity of free space, respectively. It should be noted that Eq. (3) also describes the potential variation through a sector of a sphere in which the charged particles move along radii.

If one assumes that there is no production or loss of charged particles in the space between the surfaces, then the currents of positively and negatively charged particles crossing the dotted, spherical surface in Fig. 1 will be the same as the currents drawn at the boundaries, and one may write

$$J_0 = 4\pi r^2 n_0 e u_0, \tag{3}$$

and

$$J_i = 4\pi r^2 n_i e u_i. \tag{4}$$

It should be noted that all currents in this development are treated as particle currents times the electron charge. Conventional currents associated with negatively charged particles will flow in a direction opposite to that shown in Fig. 1 and given in Eqs. (3) or (4). The total current that flows will be the sum of the two currents J_0 and J_i.

The velocities that the charged particles attain at the dotted surface in Fig. 1 are determined by the potential difference through which they have passed. Because they are assumed to have been drawn from the boundaries at zero initial velocities, these velocities are given by

$$u_0 = \sqrt{(2e/m_0)V}, \tag{5}$$

and

$$u_i = \sqrt{(2e/m_i)\,(V_i - V)}, \tag{6}$$

where m_0 and m_i are the masses of the charged particles drawn from the outer and inner surfaces, respectively. By combining Eqs. (2)–(6), the following equation is obtained:

$$\frac{d}{dr}\left(r^2\frac{dV}{dr}\right) = \frac{1}{4\pi\epsilon_0\sqrt{2e}}\left(\frac{J_0\sqrt{m_0}}{\sqrt{V}} - \frac{J_i\sqrt{m_i}}{\sqrt{V_i - V}}\right). \tag{7}$$

This equation may be simplified and put into a more tractable form for solution by nondimensionalizing it using the definitions

$$\phi = V/V_i, \tag{8}$$

$$\rho = \ln(r/r_0), \tag{9}$$

$$j_0 = (J_0/4\pi\epsilon_0 V_i^{3/2})\sqrt{m_0/2e}, \tag{10}$$

and

$$\alpha = (J_0/J_i)\sqrt{m_0/m_i} \tag{11}$$

to obtain

$$\frac{d^2\phi}{d\rho^2} + \frac{d\phi}{d\rho} = j_0\left(\frac{1}{\sqrt{\phi}} - \frac{1}{\alpha\sqrt{1-\phi}}\right). \tag{12}$$

The nondimensional boundary conditions become

$$\phi = 1 \quad \text{at} \quad \rho = \rho_i = \ln(r_i/r_0), \tag{13}$$

and

$$\phi = 0 \quad \text{at} \quad \rho = 0 = \ln(r_0/r_0). \tag{14}$$

It is noted that the problem described by Eqs. (12)–(14) is nonlinear and exhibits singularities at the two boundaries. These singularities occur because the particle densities must go to infinity at their respective source surfaces in order to satisfy the requirements of a prescribed current from each surface at zero velocity. While an analytical solution to Eqs. (12)–(14) has not been found, numerous solutions to the problem, each corresponding to different values of the nondimensional current j_0 and the nondimensional current ratio α, must exist. The solution of principal interest, however, is the space-charge-limited solution. This solution is obtained when the parameters j_0 and α are selected such that

$$\frac{d\phi}{d\rho} = 0 \quad \text{at} \quad \rho = \rho_i, \quad \text{where } \phi = 1, \tag{15}$$

and

$$\frac{d\phi}{d\rho} = 0 \quad \text{at} \quad \rho = 0, \quad \text{where } \phi = 0. \tag{16}$$

A numerical procedure will be used to solve Eq. (12) so that it meets boundary conditions (13) and (14) and so that j_0 and α are selected to yield the space-charge-limited solution, i.e., the solution that satisfies the additional conditions (15) and (16). The procedure can be simplified, however, by obtaining an equation that relates the limiting values of j_0 and α. Such an equation is obtained by multiplying Eq. (12) by $(d\phi/d\rho)d\rho$, integrating it from $\rho = \rho_i$ to $\rho = 0$ and applying conditions (15) and (16). This leads to the requirement

$$\frac{1}{\alpha} = 1 - \frac{1}{2j_0}\int_0^{\rho_i}\left(\frac{d\phi}{d\rho}\right)^2 d\rho. \tag{17}$$

The problem is solved now for a specified ratio of the radii of the spherical boundaries (r_i/r_0) by writing Eq. (12) in finite difference form and then selecting initial estimates of the outer surface space-charge-limited current density j_0 and the interelectrode potential profile $[\phi(\rho)]$. The solution to LaPlace's equation that meets boundary conditions (13) and (14) was used to obtain one initial estimate of the potential profile. Using this estimate and the assumed value for j_0, Eq. (17) was solved for α and the resulting value was used together with j_0 to determine a better estimate of the potential field using the finite difference form of Eq. (12). This relaxation process was continued until a potential field, stationary from one iteration to the next to within a small tolerance, was established. Typically the potential gradients at the boundaries associated with this solution would be nonzero. The value of j_0 was therefore changed and the relaxation technique was reapplied using the final potential profile for the previous value of j_0 as the starting potential profile for the new case. This procedure was repeated until a 0.01% increase in j_0 would result in electric fields at the boundary surface that would retard the particles leaving those surfaces. This was then taken as the final solution for the prescribed value of (r_i/r_0).

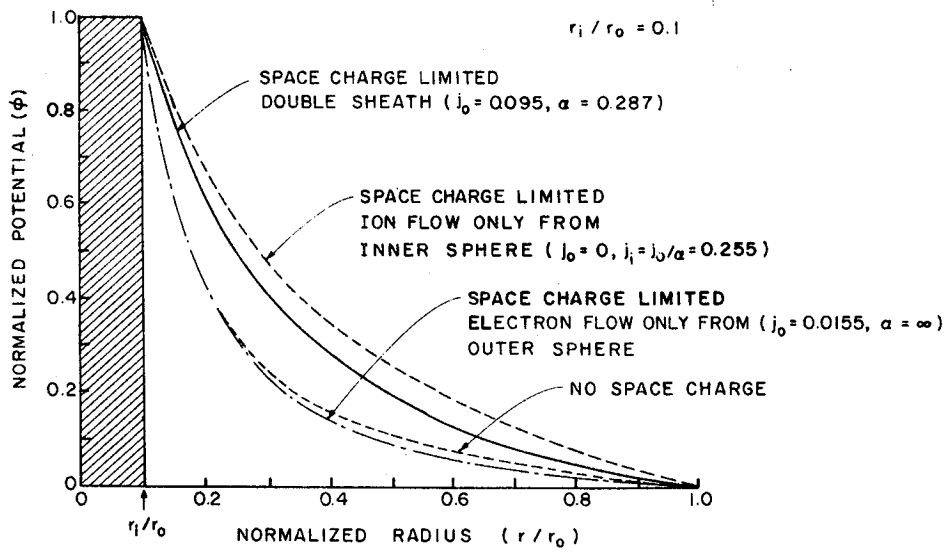

FIG. 2. Typical potential profiles.

III. VALIDATION OF NUMERICAL PROCEDURE AND RESULTS

The numerical routines used to solve the problem were tested first to determine if they would correctly solve Eq. (12) for the cases where only electrons coming from the outer sphere were present ($n_i = 0$) and only ions coming from the inner sphere were present ($n_0 = 0$). The cases correspond to the spherical single-sheath solution obtained by Langmuir.[5] Both the potential profiles and the space-charge-limited current densities determined using this procedure were found to agree with the analytical results obtained by Langmuir to within 2%.

Figure 2 shows a typical comparison of normalized potential profiles obtained for these two cases as well as for the case where no space charge is present and the case of a space-charge-limited double sheath. The dotted line shows the La-Place solution (no space charge). When electrons only are supplied at the outer surface ($r/r_0 = 1$), the potentials are lowered until they reach the space-charge limit shown as the centerline curve in Fig. 2. When ions only are supplied from the inner surface, the potentials are seen to rise above the no space-charge case. In this case the potential can be increased to the limiting value suggested by the dashed line. When the double sheath is allowed to develop (both ion and electron flow is present), the space-charge-limited potential profile represented by the solid line is obtained. Preliminary examination of the curves in Fig. 2 suggests that the zero potential gradient boundary condition at the surface of the inner sphere [Eq. (15)] may not be satisfied for the double-sheath and ion flow cases. Close examination of the data show that this condition is indeed satisfied, but the slope changes so rapidly close to the inner surface that it cannot be seen readily on the scale of Fig. 2. The potential gradients associated with the solution to the cases identified on Fig. 2 are shown in Fig. 3, and they do show that all of the potential gradient boundary conditions pertaining to each of these cases are satisfied. For the no space-charge case there is no require-

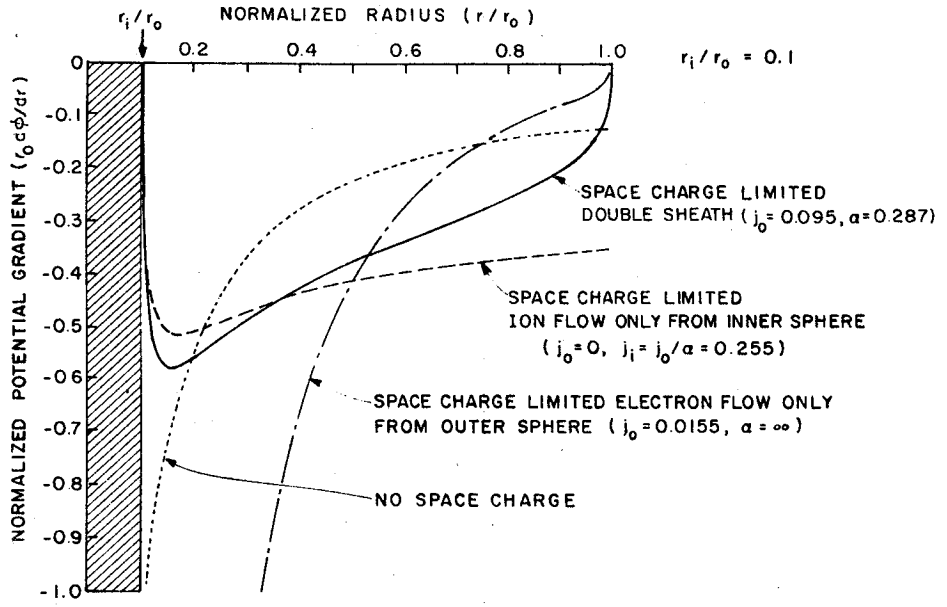

FIG. 3. Typical potential gradient profiles.

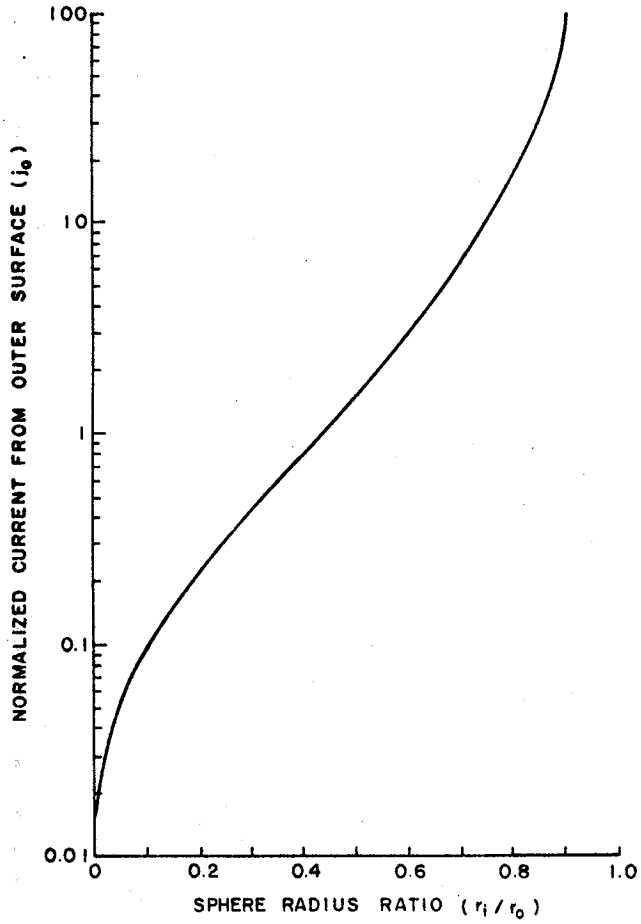

FIG. 4. Effect of radius ratio on space-charge-limited current magnitude.

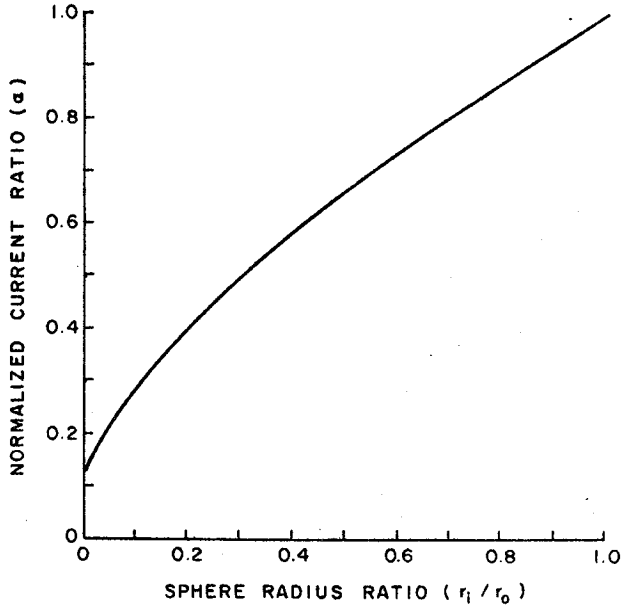

FIG. 5. Effect of radius ratio on counterflowing current ratio.

ment for zero potential gradient at either boundary, and the plots of Fig. 3 show that they are not zero. For the case of electron space-charge-limited flow from the outer sphere, Fig. 3 shows that the gradient is zero at this outer surface. For the case of positive ion space-charge-limited flow from the inner sphere, the gradient is zero at this inner surface, and an inflection point occurs at $r/r_0 = 0.175$. For the space-charge-limited double sheath the gradients at both boundaries are zero and the inflection point is observed at $r/r_0 = 0.156$.

The magnitudes of the two counterflowing space-charge-limited currents are of greater interest than the potential and potential gradient profiles shown for the double sheath in Figs. 2 and 3. These currents can be determined from the parameters j_0 and α which are defined by Eqs. (10) and (11). The values of these parameters have been computed as a function of the radius ratio (r_i/r_0) that describes the geometry of the problem, and they are given in Figs. 4 and 5. In Fig. 4 one sees that the normalized currents (j_0) are small at small radius ratios and that they become large as the radius ratio approaches unity. This wide range of normalized current variation differs from what was observed for the flat plate geometry. It occurs here because the problem has been cast in terms of radius ratio, and so the surface separation distance which was found in the planar solution does not appear in Eq. (10). In Fig. 5 the current ratio (α) is observed to approach unity with the radius ratio (r_i/r_0). This result also substantiates the validity of the numerical procedure because a radius ratio of unity corresponds to the planar case, and for this case Langmuir's analytical results[4] also yield $\alpha = 1$.

IV. APPLICATION EXAMPLE

Consider a cold, high density, argon plasma, having a radius that is 1/5 that at the spherical boundary of a lower density xenon plasma, and consider the case where the argon plasma is biased to $V_i = 50$ V positive of the xenon plasma. This model should be usable to determine the ion and electron currents that would flow between the two plasmas. In this case argon ions ($m_i = 6.7\times10^{-26}$ kg) would be expected to flow from the inner plasma surface while electrons ($m_0 = 9.1\times10^{-31}$ kg) should flow from the outer one. Using the radius ratio $r_i/r_0 = 0.2$ to enter Figs. 4 and 5 one obtains $j_0 = 0.22$ and $\alpha = 0.40$. Hence from Eqs. (10) and (11) the electron current drawn from the outer plasma boundary would be

$$J_0 = 4\pi\epsilon_0 V_i^{3/2}\sqrt{(2e/m_0)}\, j_0 = 5.1 \text{ mA},$$

and the ratio of electron-to-ion currents flowing would be expected to be

$$J_0/J_i = \alpha\sqrt{m_i/m_0} = 108.$$

V. CONCLUSIONS

Space-charge-limited, spherical double-sheath currents are determined by the radius ratio of the two surfaces involved, but are independent of the magnitudes of the radii involved. The ratio of the current drawn from the outer surface to that drawn from the inner surface varies inversely as the square root of masses of the charged particles drawn from these two surfaces. The proportionality constant in this

current ratio expression is dependent on the radius ratio and typically lies in the range ~ 0.1–1.0.

ACKNOWLEDGMENT

This work was supported by NASA under Contract Nos. NGR-06-002-112 and NAG9-120.

[1] J. E. McCoy, "Electrodynamic Tether Applications—Massive Tether Dynamics Study," NASA-JSC General Status Review, May 3, 1984.
[2] R. G. Jahn, "Basic Research for Future Electric Propulsion," AIAA Paper 85-2068, October 1985, Alexandria, VA.
[3] C. D. Child, Phys. Rev. **32**, 492 (1911).
[4] I. Langmuir, Phys. Rev. **33**, 954 (1929).
[5] I. Langmuir and K. Blodgett, Phys. Rev. **24**, 49 (1924).

DISTRIBUTION LIST

	Copies
National Aeronautics and Space Administration Washington, DC 20546 Attn:	
MT/Mr. Ivan Bekey, MS B326	1
MT/Mr. Edward J. Brazill, MS B326	1
MTF/Mr. Joseph C. Kolecki, MS B326	1
National Aeronautics and Space Administration Lyndon B. Johnson Space Center Houston, TX 77058 Attn:	
Dr. James E. McCoy, Code SN3	10
National Aeronautics and Space Administration Lewis Research Center 21000 Brookpark Road Cleveland, OH 44135 Attn:	
Mr. Michael Patterson, MS 500-220	1
Ms. Carolyn Purvis, MS 302-1	1
Mr. Frank Berkopec, MS 500-220	1
Mr. Vince Rawlin, MS 500-220	1
Department of Physics Naval Postgraduate School Monterey, CA 93943 Attn:	
Dr. Chris Olsen, Mail Code 61-OL	1
MS M0482 Martin Marietta Aerospace P. O. Box 179 Denver, CO 80201 Attn:	
Dr. Kevin Rudolph, MS M0482	1
Systems, Science and Software P. O. Box 1620 LaJolla, CA 92038 Attn:	
Dr. Ira Katz	1

Hughes Research Laboratories
3011 Malibu Canyon Road
Malibu, CA 90265
Attn:

Dr. Jay Hyman, MS RL 57	1
Dr. J. R. Beattie, MS RL 57	1

Science Applications Int'l Corp.
13400 B Northrop Way #36
Bellevue, WA 98005
Attn:

Dr. Hugh Anderson	1

Smithsonian Astrophysical Observatory
Cambridge, MA 02138
Attn:

Dr. Mario D. Grossi	1

Piano Spaziale Nazionale
Viale Regina Margherita, 202
00198 Roma, Italy
Attn:

Dr. Carlo Bonifazi	1

Istituto di Fisica dello Spazio Interplanetario
Consiglio Nazionale delle Richerche
Via G. Galilei
00044 Frascati, Italy
Attn:

Dr. Marino Dobrowolny	1
Dr. Luciano Iess	1
Mr. Luciano Vannaroni	1

Aeritalia
Societa Aerospaziale Italiana
Corso Marche 41
10146 Torino, Italy
Attn:

Dr. F. Bevilacqua	1